IEEE Access
Multidisciplinary | Rapid Review | Open Access Journal

Received 10 April 2024, accepted 11 May 2024, date of publication 17 May 2024, date of current version 3 June 2024.

Digital Object Identifier 10.1109/ACCESS.2024.3402537

RESEARCH ARTICLE

Hybrid Digital Twin Model for Greenhouse and Underground Environments

PABLO PALACIOS JÁTIVA[1], (Member, IEEE), ISMAEL SOTO[2], (Member, IEEE), CESAR A. AZURDIA-MEZA[3], (Member, IEEE), IVÁN SÁNCHEZ[4], (Member, IEEE), RIU WANG[5], AND WERTHER KERN[2]

[1]Escuela de Informática y Telecomunicaciones, Universidad Diego Portales, Santiago 8370067, Chile
[2]Department of Electrical Engineering, University of Santiago of Chile, Santiago 9170022, Chile
[3]Department of Electrical Engineering, University of Chile, Santiago 8320000, Chile
[4]Department of Telecommunication Engineering, Universidad de Las Américas, Quito 170137, Ecuador
[5]Department of Information and Communication Engineering, Tongji University, Shanghai 200070, China

Corresponding authors: Iván Sánchez (ivan.sanchez.salazar@udla.edu.ec) and Ismael Soto (ismael.soto@usach.cl)

This work was supported in part by the Project FONDECYT Iniciación under Grant 11240799; in part by the Project FONDECYT Regular under Grant 1211132; in part by STIC-AMSUD under Grant AMSUD220026; in part by Dicyt/USACH under Grant 062413SG; in part by the Escuela de Informática y Telecomunicaciones, Universidad Diego Portales; and in part by UDLA Telecommunications Engineering Degree FICA, UDLA.

ABSTRACT This research delves into the application of Digital Twins (DTs) in the realm of smart agriculture, with a particular focus on greenhouse and underground environments. By integrating computer simulations with empirical testing, we validate our hypotheses. A novel approach has been introduced that uses Visible Light Communication (VLC) for data exchange within greenhouses, along with a distinct system tailored for subterranean applications. This investigation explores how various factors influence communication effectiveness. Comprehensive testing of these systems has been conducted to evaluate their performance under a range of conditions and with varying orientations of light sources. Specifically, for our greenhouse configuration, we discovered that adjusting the system in a specific manner can substantially enhance signal quality, by nearly 10 dB at a distance of four meters, in underground scenarios. Furthermore, we have conducted evaluations using the most current WiFi and mobile networks, as well as Free Space Optics (FSO) networks, to ensure that our digital twin model is robust and capable of accurately transmitting data to a control room.

INDEX TERMS Hybrid digital twins, smart agriculture, visible light communication, greenhouse environments, underground environments.

I. INTRODUCTION

In the relentless pursuit of innovative solutions to address the specific challenges encountered in underground and greenhouse environments, it is important to mention innovative approaches based on the integration of two types of prominent technologies, Visible Light Communication (VLC) as an enabler of data communication, and Digital Twins (DTs) for analysis, processing, and optimization of these received data. Based on this context, its application in these unconventional environments, characterized by extreme environmental conditions and unique operational requirements, demands advanced technological strategies to improve efficiency, safety, and monitoring of critical processes.

Visible Light Communication (VLC) has emerged as a promising technology for data transmission in challenging environments that offers significant advantages over conventional radio-frequency technologies. The ability of visible light to operate under adverse conditions, such as the presence of dust, humidity, and structural obstacles, makes it an attractive option for communication in underground environments, where space restrictions and electromagnetic interference are critical concerns.

The associate editor coordinating the review of this manuscript and approving it for publication was Julien Sarrazin.

© 2024 The Authors. This work is licensed under a Creative Commons Attribution-NonCommercial-NoDerivatives 4.0 License.
For more information, see https://creativecommons.org/licenses/by-nc-nd/4.0/

As industries increasingly navigate complex and dynamic environments, the first facet of VLC system implementation proposals revolves around understanding and harnessing the potential of visible light communication. Taking advantage of the inherent characteristics of light, this technology not only offers a viable alternative to traditional communication methods, but also opens avenues for improving reliability and performance under the difficult conditions typical of underground and greenhouse environments.

However, VLC is not without its own set of challenges. One notable hurdle is the limited range inherent in visible light, which can pose difficulties in large and complex environments such as underground mines or greenhouses. Additionally, the effectiveness of VLC can be impacted by factors such as variable light conditions and the need for a Line-of-Sight (LoS) communication path. Overcoming these challenges is critical to the successful deployment of VLC in these environments.

Expanding on the potential of VLC, the second facet of a complete solution delves into the realm of DTs, an emerging innovation in the field of computing. DTs offer a unique platform to simulate and optimize complex processes. The ability to manipulate information through DTs presents new possibilities for accurately modeling mining and greenhouse environments, enabling more informed decision making and efficient resource management.

DTs, as a cutting-edge facet of this research, introduce a paradigm shift in computational capabilities. These DTs have the potential to perform intricate computations at speeds unimaginable with classical computing systems. This advantage not only opens avenues for accelerated simulations, but also holds the promise of uncovering nuanced patterns and correlations within the complex dynamics of UM and greenhouse ecosystems.

As we explore the potential applications of DTs in these environments, it becomes essential to acknowledge the inherent challenges associated with computing technologies. One of the primary challenges is the issue of coherence and error correction. The fragile nature of states makes them susceptible to interference, necessitating sophisticated error-correction mechanisms to maintain the integrity of computations. Additionally, the current practical implementation of computing is still in its infancy, with scalability and stability being significant concerns. Overcoming these challenges is imperative to fully exploit the capabilities of DTs in real-world scenarios, ensuring their viability as a transformative tool for precise environmental modeling and decision support.

This paper introduces a hybrid twin model that takes advantage of the complementary strengths of VLC, and data transmission via VLC can enhance the ability of DTs to simulate and optimize intricate environments. Furthermore, we evaluated the applicability of this approach in underground and greenhouse scenarios, identifying specific use cases, and evaluating its performance under real-world conditions.

As we advance toward a smarter and more adaptable technological future, this work aims to lay the groundwork for the practical implementation of hybrid solutions that enhance operability and sustainability in challenging environments such as UM and greenhouses. Through the strategic convergence of VLC and DTs, we seek to contribute to the realization of more intelligent and resilient systems for these demanding scenarios.

The manuscript has the following organization. Section II presents a review of advances and challenges in modern agriculture using greenhouses and underground tunnels, Section III presents the hybrid DT system model, Section IV proposes the greenhouse VLC system and theoretical channel model. Section V establishes the theoretical UM-VLC channel model, Section VI shows the results and analysis. Finally, Section VII is dedicated to conclusions based on the results obtained and future work.

II. RELATED WORK

A. ADVANCES AND CHALLENGES IN MODERN AGRICULTURE USING GREENHOUSE

The initial advancements, marked by the study of Shang et al. [1], introduced the use of ZigBee technology in Wireless Sensor Networks (WSNs) for greenhouse monitoring, representing a significant step toward automation and remote monitoring, despite the absence of complex mathematical models for communication.

The transformative potential of Digital Twins (DTs) in smart agriculture, explored by Verdouw et al. [2], and the focus on virtualization of cultivation processes in greenhouses [3], signal a move towards more sophisticated and sustainable agricultural management systems. The application of DTs in agriculture emphasizes the importance of robust design frameworks and the adaptability of these technologies to real world scenarios, as demonstrated in the European IoF2020 project [2].

Research by Jans-Singh et al. [4] on DTs in urban hydroponic systems and the study by Slob and Hurst [5] on the use of Industry 4.0 technologies in greenhouses highlight the optimization of resource use and the improvement of energy efficiency as central challenges, despite technological advancements. The development of frameworks for the optimal design of agrophotovoltaic solar farms [6] and the analysis of the controls of the thermal environment in vertical farming [7] reflect a focus on the integration of renewable energies and sustainability, underlining the continuous search for a balance between productive efficiency and minimization of environmental impact.

Technologically, the introduction of GSM and WSN-based systems for greenhouse monitoring by Aher et al. [8], and the development of smart lighting prototypes using narrowband IoT technology by Chang et al. [9], illustrate progress in greenhouse connectivity and environmental management. However, these advances highlight the need for a deeper exploration of propagation models and analysis of the

performance of the physical layer to optimize communication efficiency.

Mittal et al. [10] and Sotner et al. [11] introduce innovations in the management of essential agricultural parameters and in low-bit-rate communication for agricultural applications, respectively, highlighting the importance of energy efficiency and effectiveness in the transmission of critical information. Geng et al. [12] advance the development of mobile IoT systems for greenhouse monitoring, demonstrating the usefulness of sophisticated system architectures for data acquisition and motion control. This innovative approach highlights the need for detailed signal behavior analysis and propagation models to fully assess communication systems in agricultural environments.

Finally, the study by Ghassemlooy et al. [13] on the implementation of LoRa-based technologies underscores the challenges and limitations of IoT connectivity in greenhouses, paving the way for the exploration of alternative and energy-efficient communication technologies such as VLC. Information can be uploaded or downloaded using LoRa for radio or light within the greenhouse or underground tunnel. Additionally, WiFi, 5G, or FSO can be used depending on the distances between the hub and the DT.

This review of the literature highlights a common theme: all studies are dedicated to developing monitoring and communication solutions for greenhouses and agricultural settings, primarily using technologies such as ZigBee, GSM, IR and various RF-based systems. In particular, as discussed previously, there is evidence suggesting that electromagnetic fields and RF technologies can adversely affect crop health. Furthermore, our review reveals a notable gap in existing research, particularly the lack of exploration into environmentally friendly or alternative technologies tailored for communication in agronomic greenhouse environments. This identified gap presents a unique research opportunity for us to introduce a pioneering communication approach using VLC. Our focus will be on characterizing the specific channel model for VLC, positioning it as a potentially more suitable and sustainable option for agricultural applications.

Similarly to the previous discussion of underground channels, limited research has been conducted on the use of VLC in agricultural greenhouses. This lack of exploration presents an opportunity to explore and implement a wider range of communication channels in this context.

Information can be uploaded or downloaded using LoRa for radio or light within the greenhouse or underground tunnel. In addition, WiFi, 5G, or FSO can be used depending on the distances between the hub and the DT.

B. ADVANCE AND CHALLENGES IN MODERN AGRICULTURE USING UNDERGROUND TUNNELS

The historical evolution of the Internet of Underground Things (IoUT) reflects a journey marked by significant technological advances that aim to overcome the unique challenges of underground communication. This evolution has been propelled by the combined efforts of researchers and technologists, as evidenced by a series of pivotal studies.

The discourse began with Saeed et al. [14], highlighting recent advances in IoUT, with a focus on communication technologies, networking issues, and localization techniques. This foundational work explored a range of wireless and wired communication technologies to navigate the challenges posed by the underground environment, finding applications in the oil and gas, agriculture and seismic mapping sectors. The study underscored the potential of IoUT to revolutionize data collection and monitoring in subterranean settings.

Building on these insights, Vuran et al. [15] delved into communication architectures specifically designed for precision agriculture within the IoUT framework. This research emphasized the integration of underground sensors, machinery, and irrigation systems, bridging these technological components with the broader social network of agricultural stakeholders. It showcased advances in underground wireless communication while addressing the design and implementation challenges inherent in IoUT systems.

In a leap towards optimizing IoUT's operational efficiency, Esmaiel et al. [16] introduced a deep learning-based index modulation technique adapted for underground communications. This innovative approach aimed to improve both spectral and energy efficiency, address inefficiencies prevalent in existing IoUT technologies, and thus mark a significant step forward in the refinement of IoUT performance in challenging environments.

Drawing inspiration from nature, Zhong et al. [17] developed a bio-inspired vibrational wireless underground communication system. Mimicking subterranean animals, this system utilized a bio-inspired source and MEMS accelerometers, among other components, to demonstrate effective data transmission within the IoUT, showcasing the potential of biomimicry in overcoming technological hurdles.

Addressing the physical aspects of IoUT infrastructure, Salam et al. [18] proposed a theoretical model for underground dipole antennas, with a particular focus on the impact of soil moisture on antenna performance. Through empirical evaluations and simulations, this work provided valuable insights into the design of efficient communication systems for IoUT, highlighting the critical nature of environmental factors in the design of the system.

With an eye towards precision in environmental monitoring, Bertocco et al. [19] proposed an augmented sensing method to estimate the volumetric water content of the soil within IoUT contexts. By marrying machine learning algorithms with sensor data and signal strength indicators, this approach demonstrated a notable improvement over traditional sensing methods, offering a path towards more accurate and reliable environmental data collection.

Further refining the technological toolkit for IoUT, Skiljo et al. [20] focused on optimizing antenna design for soil moisture sensing. Advocating for a narrowband antenna design, this research highlighted the discernible signal level differences in varying moisture conditions, which could

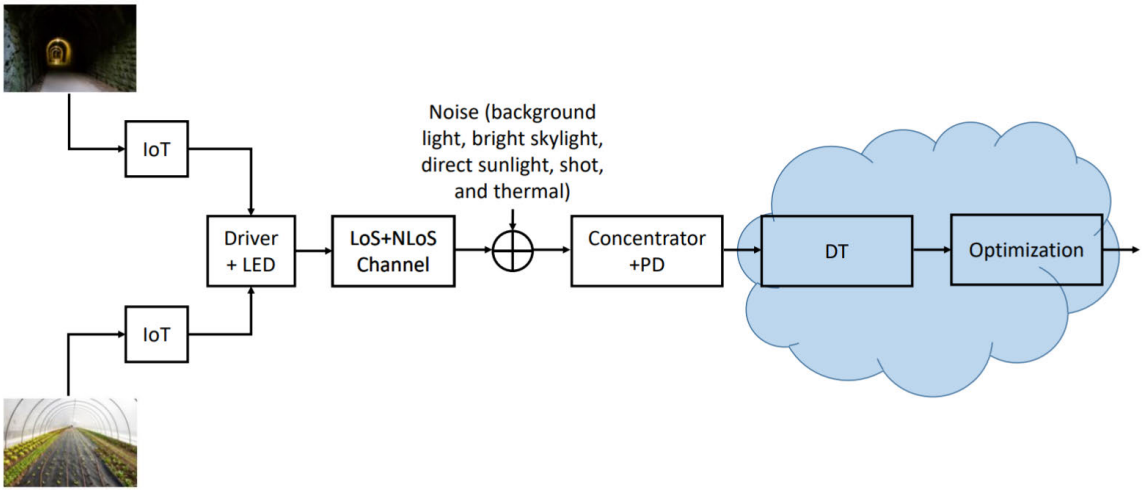

FIGURE 1. General diagram of a DT with VLC.

improve the reliability of radio sensing techniques for soil moisture measurement.

Despite these advancements, the exploration of VLC within the context of underground agriculture remains uncharted territory. This gap presents an opportunity for future research to diversify the IoUT ecosystem further, leveraging VLC's unique properties to enhance underground communication solutions. The historical progression of IoUT research underscores a dynamic field poised for continued innovation, with the potential for VLC to introduce a new dimension to underground agricultural practices.

Although there is a great deal of work in underground environments, there are no articles on underground agriculture using VLC, which could be innovative and lead to a more diverse system.

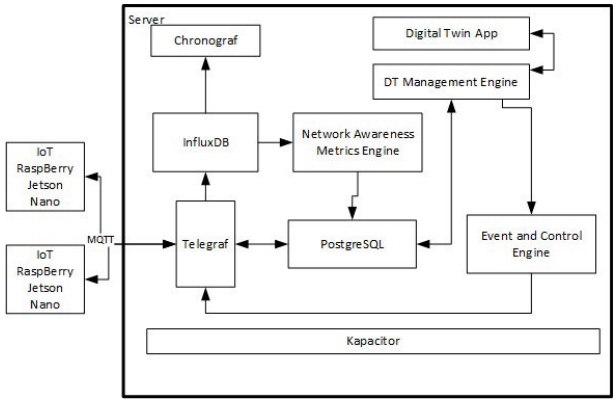

FIGURE 2. Twin architecture.

III. GENERAL MODEL OF SENSOR-ENABLED HYBRID DIGITAL TWIN

DTs represent a formidable solution to transform existing systems into intelligent frameworks capable of addressing a myriad of challenges, including environmental concerns, production inefficiencies, and labor shortages. Despite its potential, the world of precision agriculture has yet to fully leverage the capabilities of DT. Thus, any effort aimed at integrating these innovative concepts could significantly facilitate their adoption within an infrastructure that leverages various IT solutions. In this section, we dive into the conceptual and theoretical foundations to illustrate the viability of employing sensors within an underground tunnel to create a DT-enabled environment. This setup will serve as a platform to demonstrate applications such as predicting greenhouse temperatures across different settings and showcasing the practical benefits and potential of DTs in enhancing agricultural practices.

A. DIGITAL TWIN MODELS ADAPTED TO SMART FARMING

Previous studies have provided detailed documentation of various case studies that have successfully implemented this concept within the agricultural sector, focusing on crops [2]. Digital Twins (DTs) are utilized as predictive systems for forecasting outcomes in specific crops, including tomatoes and lettuce, and in some instances, to simulate the operation of specialized agricultural equipment, such as weed cutters. Predominantly, these case studies leverage DTs to monitor the present condition of objects and to predict their future states accurately.

In Fig. 1, the link to a tunnel or a greenhouse is shown. Because the goal may be to remotely control one or more LEDs or the operation of a fan, it is necessary to use messaging queues to carry out this task, as it is through Message Queuing Telemetry Transport (MQTT) that the actions to be performed are sent.

Another rapidly emerging concept in the realm of communications is 5G technology, known for its advances in minimizing latency and improving connection speeds. Although there are currently limited instances of IoT combined with 5G networks, this integration has the potential to significantly enhance the capabilities of a DT system in the future. The work of [21] stands as a noteworthy example of progress in the merging of IoT and 5G technology.

In Fig. 2, the VLC channel is not represented, it only shows what data collection refers to, and the use of the ICT stack is implemented, including Chronograf to visualize the collected information, as well as communication between Influxdb and Telegraf. The benefit of this lies in the fact that Influxdb, being a time series database, stores only the timestamp, the data source, and the data itself. While Chronograf allows visual monitoring of the data, in practice, a set of codes has been developed to execute actions, with InfluxDB serving as a database. On the other hand, communication at a layer closer to the physical layer is carried out through the MQTT messaging protocol [22].

The code that governs the aforementioned processes is embedded in the Jetson nano with Graphics Processing Unit (GPU), which reads from and writes to the process. It not only facilitates edge computing but also transmits measurement data to the database for machine learning purposes. The mathematical model developed for temperature prediction uses the dataset created by the digital twin, with a detailed explanation provided in Section III-B.

Radio signal-based systems use electromagnetic waves of the radio frequency spectrum to locate mobile nodes. They offer two key services: aiding in position estimation and enabling wireless information transmission for mobile node mobility. However, these systems face unique challenges in underground mines due to the different behavior of radio frequency (RF) signals in mine tunnels. The tunnel's physical shape can cause signal scattering, multi-path propagation, and blockage. Furthermore, tunnel walls vary in material composition and affect signal propagation due to their unique electromagnetic characteristics. Other technologies are the following: Wireless Local Area Networks (WLAN): WLAN (IEEE 802.11) is established in various sectors. It uses ISM bands in 5 and 2.4 GHz for full-duplex wireless communications, offering data transmission rates between 1 and 108 Mbps and coverage up to 150 meters. WLAN can support various position estimation methods and does not require line of sight for data transmission.

Radio Frequency Identification (RFID): RFID systems store and retrieve data using radio waves. They consist of RFID readers and tags (passive, semi-passive, and active). The deployment of RFID systems is specific and strategic due to their short coverage range.

Wireless Personal Area Networks (WPAN): WPANs, such as Bluetooth and ZigBee, have been extensively investigated in underground environments. They provide bi-directional wireless communications but with shorter coverage ranges than WLAN and lack pre-deployed infrastructure. Each WPAN standard differs in its physical layer properties.

Ultra Wide Band (UWB): UWB is notable for its high accuracy in localization systems due to precise time-of-flight range estimation. It operates across a broad frequency range and is considered promising for WPAN applications and sensor networks.

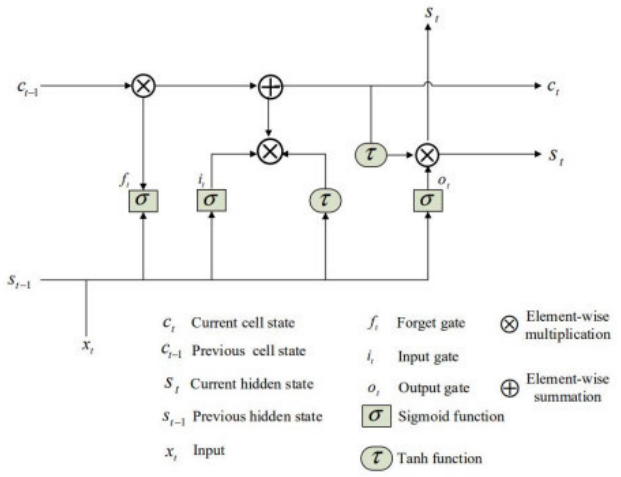

FIGURE 3. LSTM architecture.

The text emphasizes the unique requirements and challenges of implementing these technologies in greenhouse and underground mines, considering factors such as signal propagation, environmental conditions, and the need for specific infrastructure adaptations.

B. LSTM (LONG-SHORT TERM MEMORY NEURAL NETWORKS)

Introduced by Hochreiter in 1997 [23], LSTMs are a specialized form of Recurrent Neural Networks (RNNs), crafted to capture and learn from long-term dependencies within data. Each neuron in an LSTM network acts as a memory cell equipped with three gates: an input gate, a forget gate, and an output gate. These gates collectively manage the flow of information across different time steps, ensuring that the network can maintain and update its internal state appropriately. Unlike traditional neural networks, where neurons generate a single output value, LSTM cells produce two outputs: the cell state c_t, which serves as long-term memory, and the hidden layer output s_t. This dual output mechanism is crucial for LSTMs' ability to preserve information over long sequences without losing significance in earlier inputs, addressing the gradient diminishment issue inherent to standard RNNs. For temperature prediction, the LSTM neural network model is employed as the primary approach.

For a better understanding of how LSTM networks function and for a more detailed description, refer to the research paper by Tran et al. [24].

Fig. 3 illustrates a schematic of the main operation in the cells of LSTM networks. In the first stage of LSTM, it is decided which data will be discarded from the cell in the current state. The forget gate f_t makes this choice according to equation 1.

$$f_t = \sigma\left(W_{fx}x_t + W_{fx}s_{t-1} + b_f\right), \tag{1}$$

where σ is the sigmoid function, x_t is the input signal, s_{t-1} is the previous hidden state, and W_{fx} and b_f are the weight matrices and the bias of forget gate. The next step is to decide

what new information will be stored in the cell state. There are two tasks involved here; first, the input gate i_t decides which values will be updated, and second, a hyperbolic tangent layer (tanh) creates a vector of new values to be applied ($\widetilde{c_t}$), as shown in equations 2 and 3, respectively.

$$i_t = \sigma\left(W_{ix}x_t + W_{ix}s_{t-1} + b_i\right), \tag{2}$$

$$\widetilde{c_t} = \tanh\left(W_{\bar{c}x}x_t + W_{\bar{c}x}s_{t-1} + b_{\bar{c}}\right), \tag{3}$$

where (W_{ix}, b_i) and $(W_{\bar{c}x}, b_{\bar{c}})$ are the weight matrices and the biases of input gate and memory cell state, respectively. Then, the old cell state c_{t-1} is updated to the new cell state c_t, as given by equation 4.

$$c_t = f_t \otimes c_{t-1} + i_t \otimes \widetilde{c_t}, \tag{4}$$

where $\otimes$ is the multiplicative operator. Finally, in equation 5 the output gate o_t decides which components of the cell state will be output. The cell goes through a tanh layer and is multiplied by a cross product as shown in equation 6.

$$o_t = \sigma\left(W_{ox}x_t + W_{ox}s_{t-1} + b_o\right), \tag{5}$$

$$s_t = o_t \otimes \tanh\left(c_t\right), \tag{6}$$

where W_{ox} and b_o are the weight matrix and the bias of the output gate. A more detailed explanation of the results is provided in Section VI-M.

IV. GREENHOUSE VLC SYSTEM AND THEORETICAL CHANNEL MODEL

Fig. 1 shows the method for transmitting or receiving data using LoRa for radio or light-based communication within a greenhouse or an underground tunnel. When the distance between the concentrator and the DT extends beyond the effective range of LoRa, it is advisable to employ alternative communication technologies such as WiFi, 5G, or FSO. To ensure efficient and high-priority communication in agronomic environments, such as greenhouses or tunnels, it is essential to effectively manage light distribution. To address this, an array of LEDs is installed throughout the greenhouse, serving the dual purpose of providing illumination and facilitating communication. Strategic placement of LEDs, especially at the curved junctures where the walls and ceiling converge, as shown in Fig. 4, is particularly effective. This positioning not only simplifies the installation and maintenance of LED systems, but also maximizes their utility in these agricultural settings. In this study, we use the geometric layout of a VLC downlink transmission to examine an agronomic greenhouse scenario shown in Fig. 4. We will talk about all its variables and constants in the sections that follow. We will consider a section of the greenhouse for analysis. This section is equipped with LED transmitters and, to optimize the communication effect, the intensity of the light in the greenhouse should be distributed as evenly as possible. Therefore, multiple LEDs must be installed throughout the greenhouse.

The VLC channel is the space between the LED and the PD, and to model it, three different components must be analyzed: LEDs with the orientation-based LED model, PDs with the non-imaging photo-detector model, and the optical propagation model.

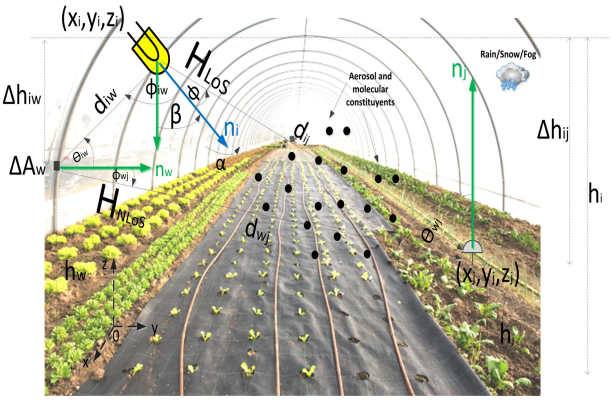

FIGURE 4. The geometry of the LoS and non-LoS propagation model in the agronomic greenhouse.

A. ORIENTATION-BASED LED AND NON-IMAGING PHOTO-DETECTOR MODELS

To mathematically model the orientation of the LED in the greenhouse, we define ϕ_g as the angle of radiation related to the normal vector $\boldsymbol{n}_i$ of the position of the LED and its position in the greenhouse as (x_i, y_i, z_i) in the Cartesian coordinate system, where $i = 1, 2, \ldots, I$ and I is the total number of LEDs.

As mentioned above, in greenhouses, the LEDs do not point vertically downward because of their orientation. Therefore, it must be described from two separate angles. These angles are defined as the tilt angle with respect to the z-axis, which is represented by β and takes values in the range of $[-90°, 0°)$, and the rotation angle with respect to the x-axis, which is indicated by α and defined in the interval $[0°, 180°)$. The ranges of values were adjusted to the real physical characteristics that the LED orientation can take in the greenhouse.

Assuming that each LED has the same generalized Lambertian radiation pattern, and since this model is widely used for the light emission distribution of the LEDs [13], [25], the radiation intensity pattern $S(\phi_g)$ is given as [13], [25]

$$S(\phi_g) = \begin{cases} \dfrac{m+1}{2\pi}\cos^m(\phi_g) & \text{if } \phi_g \in [-\dfrac{\pi}{2}, \dfrac{\pi}{2}] \\ 0 & \text{otherwise} \end{cases}, \tag{7}$$

where ϕ_g is the irradiance angle of LED. It is evident that the orientation of the LED affects ϕ_g and is distinguished specifically in the term $\cos(\phi_g)$, which, based on vector concepts, is defined as follows:

$$\cos(\phi_g) = \frac{V_{i-j} \cdot \boldsymbol{n}_i}{\|V_{i-j}\|\|\boldsymbol{n}_i\|}. \tag{8}$$

In this context, the vector from a LED to a PD is represented by V_{i-j}, the 2-norm is denoted by $\|\cdot\|$, and the operation of the dot product is represented by $\cdot$.

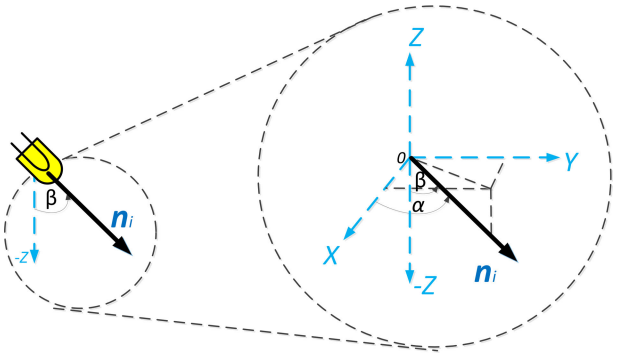

FIGURE 5. LED position and orientation features.

Furthermore, for vector concepts, the magnitude of $\|V_{i-j}\|$ is equal to d_{ij}, which corresponds to the Euclidean distance between the LED and the PD. The magnitude of $\|\boldsymbol{n}_i\|$ is 1, and $\boldsymbol{n}_i$ can be expressed in terms of α and β as $\boldsymbol{n}_i = [\sin(\beta)\cos(\alpha), \sin(\beta)\sin(\alpha), -\cos(\beta)]$. Notice that the z-component of $\boldsymbol{n}_i$ is negative since the LED is pointing downward. Furthermore, $V_{i-j} = \left[x_j - x_i, y_j - y_i, -\Delta h_{ij}\right]$, where the position of the PD is represented by (x_j, y_j, z_j) in the Cartesian coordinate system and assuming that Δh_{ij} is the height difference between the LED and the PD, that is, z_i-$z_j = \Delta h_{ij}$. Consequently, the expression (8) can be rewritten in the following form:

$$\cos(\phi_g) = \frac{\left[x_j - x_i, y_j - y_i, -\Delta h_{ij}\right]}{d_{ij}} \cdot [\sin(\beta)\cos(\alpha), \sin(\beta)\sin(\alpha), -\cos(\beta)]\,. \quad (9)$$

The Cartesian position and the elementary angles that make up the orientation of the LED are represented in Fig. 5.

For this agronomic greenhouse scenario, we assume that the PDs are installed in the soil above the sensors that control the functions that will be applied to the crops. Thus, PD is assumed to be fixed and vertically oriented upward, where its position is represented by (x_j, y_j, z_j) in the Cartesian coordinate system with $j = 1, 2, \ldots, J$ and J is the total number of PD.

The effective collection area of the PD acquires the form of [13], [25]

$$A_{eff}(\theta_g) = \begin{cases} A_p \cos(\theta_g) & \text{if } -\Theta/2 \le \theta \le \Theta/2 \\ 0 & \text{otherwise} \end{cases}, \quad (10)$$

where θ_g is the incidence angle with respect to the normal vector $\boldsymbol{n}_j$ of the PD position.

B. THEORETICAL CHANNEL MODELING FOR VLC IN AGRONOMIC ENVIRONMENTS

In general, VLC channel models feature two main optical components: the LoS component and the NLoS component. These components vary depending on factors such as the location of the PD in the greenhouse and the distance between the LED and the PD, among others. In this manuscript, the LoS component is directly a result of the LED lighting falling on the PD. Therefore, the LoS link depends on the parameters of the LEDs and PDs. The DC gain of the LoS optical wireless channel is formulated by merging expressions (7) and (10) as follows [13], [25]:

$$H^g_{LoS}(0) == \frac{(m+1)A_p}{2\pi d_{ij}^2} \cos^m(\phi_g)\cos(\theta_g)G(\theta_g)rect\left(\frac{\theta_g}{\Theta}\right), \quad (11)$$

where $rect\left(\frac{\theta_g}{\Theta}\right) = 1$ for $0 \le \theta \le \Theta$ and 0 otherwise, d_{ij} is the Euclidean distance between the LED and PD, and $G(\theta_g)$=$T_s(\theta_g)$ $g(\theta_g)$ represents the combined gain of the optical filter and optical concentrator, respectively.

As explained in Section IV-A, we consider a variable and random LED orientation. Therefore, we can integrate the expression (9) into the derived LoS channel component, obtaining the following expression:

$$H^g_{LoS}(0) = \frac{(m+1)A_p}{2\pi d_{ij}^{m+2}} \left[x_j - x_i, y_j - y_i, -\Delta h_{ij}\right]^m \cdot [\sin(\beta)\cos(\alpha), \sin(\beta)\sin(\alpha), -\cos(\beta)]^m \cos(\theta_g) \times G(\theta_g)rect\left(\frac{\theta_g}{\Theta}\right). \quad (12)$$

However, although there are fewer or no obstacles in a greenhouse, it is possible to create a diffuse optical component by reflecting light on the walls or ceiling. The sum of all the generated reflections arriving at the PD generates an NLoS component of the VLC channel. For simplicity and similarity of scenarios, we assume that this component can be modeled as equation 25. d_iw and d_wj, respectively, provide element w and the PD.

As we have mentioned, to present a complete VLC channel model applicable to agronomic greenhouse environments, we must consider all the factors that affect these scenarios. These factors will be conceptualized in Section IV-C that follows.

C. ATMOSPHERIC FACTORS INTEGRATED INTO THE VLC CHANNEL MODEL FOR AGRONOMIC GREENHOUSES.

In an agricultural greenhouse, environmental factors can cause optical links to lose their signal in a way that is very similar to how RF channels (microwave and millimeter) lose their signal. However, in optical links, the fading is greater than in RF signals. The optical signal propagating through a free space channel is susceptible to atmospheric conditions such as fog, rain, and sun, among others.

For optical radiation traveling through the VLC channel, the interaction between photons (light beams) and the molecular constituents of the atmosphere makes some of the photons extinguish while other photons are scattered. The Beer-Lambert law (BLL) is a model that can explain these events. The BLL law describes a mathematical model to represent the absorption and scattering of light through the atmosphere. These factors, combined, reduce the PD's received power and must be included in the VLC channel model.

For our modeling purposes, we introduce the exponential BLL as a function of the distance between the LED and the PD, as follows:

$$\tau(d_{ij}) = e^{-\gamma(\lambda)d_{ij}}, \tag{13}$$

where $\gamma(\lambda)$ is the extinction coefficient per unit of length with wavelength λ.

As we explained earlier, the attenuation of the optical signal in the greenhouse environment is due to the scattering and absorption introduced by gases and aerosols. Aerosol comprises small particles of various shapes ranging from spherical to irregular forms suspended in the atmosphere. In general, $\gamma(\lambda)$ can be expressed as

$$\gamma(\lambda) = \alpha_m(\lambda) + \alpha_a(\lambda) + \beta_m(\lambda) + \beta_a(\lambda), \tag{14}$$

where α_m and α_a are the absorption coefficients for the molecular and aerosol, respectively, and β_m and β_a are the scattering coefficients for the molecular and aerosol, respectively.

These coefficients can be varied and adapted according to the atmospheric factors that affect the agronomic greenhouse. The next step is to integrate them into the VLC channel model, both for the LoS component (expression 12) and for the NLoS component (expression 25), rewriting them as follows:

$$\begin{aligned} H^g_{LoS}(0) = {} & \frac{(m+1)A_p}{2\pi d_{ij}^{m+2}} \left[x_j - x_i, y_j - y_i, -\Delta h_{ij}\right]^m \\ & \cdot \left[\sin(\beta)\cos(\alpha), \sin(\beta)\sin(\alpha), -\cos(\beta)\right]^m \\ & \times \cos(\theta) G(\theta) \text{rect}\left(\frac{\theta}{\Theta}\right) \tau(d_{ij}), \end{aligned} \tag{15}$$

$$\begin{aligned} H_{NLoS}(0) = {} & \frac{(m+1)A_p}{2\pi} \sum_{w=1}^{W} \frac{\Delta A_w \rho_w}{d_{iw}^2 d_{wj}^2} \cos^m(\phi_{iw}) \cos(\theta_{iw}) \\ & \times \cos(\phi_{wj}) \cos(\theta_{wj}) G(\theta_{wj}) \text{rect}\left(\frac{\theta_{wj}}{\Theta}\right) \\ & \times \tau(d_{iw}) \tau(d_{wj}). \end{aligned} \tag{16}$$

Finally, the total DC gain for the VLC channel applied to agronomic greenhouses is the sum of the LoS and NLoS components, namely,

$$H_{greenhouse}(0) = H^g_{LoS}(0) + H_{NLoS}(0). \tag{17}$$

D. OPTICAL PROPAGATION MODEL IN AGRONOMIC ENVIRONMENTS

The VLC system applicable to agronomic greenhouses can be modeled like any wireless communication system, considering the input optical signal $X(t)$ and the output optical signal $Y(t)$. Furthermore, due to the lighting characteristics that greenhouses must have, multiple LEDs and PDs are distributed in the scenario. For that reason, here is the equivalent base-band model we use to talk about a VLC intensity modulation/direct detection (IM/DD) system for agricultural greenhouses:

$$Y(t) = R_{PD}\xi X(t) \otimes h_{greenhouse}(t) + N(t), \tag{18}$$

where ξ is the LED modulation index, $h_{greenhouse}(t)$ is the VLC channel impulse response of the greenhouse environment, and $\otimes$ is the convolution operator. An important point to consider in our work is noise. Many outside noise sources can affect VLC applications in agronomic greenhouses, so these need to be taken into account in the full propagation model. Therefore, we establish $N(t)$ as additive noise in PD, including background light and bright skylight noises. There are other background noise sources on the receiver side, such as thermal noise, which are generated in the components of the receiver's electronic circuit, such as resistors and capacitors. To roughly estimate the total noise on the receiver side, use the formula

$$\begin{aligned} \sigma^2_{total} = {} & 2qrP^g_r B_n + 2qP_a B_n + \frac{8\pi\kappa T_k}{G}\eta A_p I_2 B_n^2 \\ & + \frac{16\pi^2\kappa T_k \Gamma}{g_m} C^2_{pd} A_p^2 I_3 B_n^3. \end{aligned} \tag{19}$$

The first term corresponds to photon fluctuation noise or quantum noise, where q is the electric charge constant, and B_n is the bandwidth of the electrical filter that follows the PD. Here, P^g_r is the power received by the PD due to the light emitted by the LED P^g_t, which is expressed as

$$P^g_r = P^g_t H_{greenhouse}(0). \tag{20}$$

The second term of the expression (19) corresponds to the dark current and excess noise, where P_a is the ambient light power detected by the receiver expressed as

$$P_a = P_{bg}\Delta\lambda A_p I_2, \tag{21}$$

where P_{bg} is the background irradiance per unit bandwidth, $\Delta\lambda$ is the filter bandwidth, and I_2 is the noise bandwidth factor. Finally, the third and fourth terms of the expression (19) represent feedback resistor noise and field effect transistor (FET) channel noise, respectively. Here, κ is Boltzmann's constant, T_k is absolute temperature, G is the open-loop voltage gain, C_{pd} is the fixed capacitance of PD per unit area, Γ is the FET channel noise factor, g_m is the FET transconductance, and I_3 is the noise bandwidth factor.

As we mentioned, this work aims to study, characterize, and derive a mathematical model for the VLC channel in the environment of agronomic greenhouses. The analysis established in this section allowed us to derive expression (17), complying with the initial premise.

V. UNDERGROUND VLC SYSTEM AND THEORETICAL CHANNEL MODEL

A. LIGHT PROPAGATION MODEL

In an underground scenario, the power received (P_r) in any optical receiver (R_x) arranged in the scenario is given by [26]

$$P_r = P_t R_{PD}\left(H_{LoS} + H_{NLoS}\right) + N_t, \tag{22}$$

where R_{PD} represents the PD responsivity, H_{LoS} denotes the DC channel gain component of the Line-of-Sight (LoS) link, and H_{NLoS} represents the DC channel gain component

of the Non-Line-of-Sight (NLoS) link. The additive noise component, denoted N_t, is a combination of thermal and shot noises [27]. It is important to note that the DC channel gain of the LoS component is influenced by the position and orientation of both the optical transmitter (T_x) and R_x. Therefore, the representation of the DC channel gain for the LoS component can be expressed as follows [26], [28]:

$$H_{LoS} = \frac{A_p(m+1)}{2\pi d^2}\cos^m(\phi)\cos(\theta)T_s(\theta)g(\theta)rect(\frac{\theta}{\Theta}), \quad (23)$$

the symbol A_p represents the physical area of the PD. The parameter m corresponds to the Lambertian mode number. The distance between T_x and R_x is denoted as d in Euclidean terms. The variable ϕ denotes the irradiance angle of T_x, while θ represents the incidence angle in R_x. The function $g(\theta)$ represents the gain of the optical concentrator. The symbol Θ denotes the Field of View (FoV) of R_x. Lastly, $rect(\cdot)$ corresponds to a decision function. In turn, the CIR of the LoS component is represented as follows:

$$h_{LoS}(t) = \frac{A_p(m+1)}{2\pi d^2}\cos^m(\phi)\cos(\theta)g(\theta)rect(\frac{\theta}{\Theta})\delta(t-\frac{d}{c}), \quad (24)$$

where c denotes the velocity of light, and $\delta(\cdot)$ represents Dirac's function, which signifies the delay in signal propagation.

The presence of the NLoS component is a result of light being reflected. This reflection typically occurs when light comes into contact with the walls of the tunnel. The Lambertian reflectance model is often used to explain these reflections, where light is reflected with the same intensity in all directions. Thus, when considering T_x and R_x in an underground scenario, the DC channel gain of the NLoS component can be expressed as the accumulation of these reflections [26], [28]:

$$H_{NLoS} = \frac{A_p(m+1)}{2\pi}\sum_{w=1}^{W}\frac{\Delta A_w \rho_w}{2\pi d_{tw}^2 d_{wj}^2}cos^m(\phi_{tw})cos(\theta_{tw})cos(\phi_{wr}) \times cos(\theta_{wr})T_s(\theta_{wr})g(\theta_{wr})rect(\frac{\theta_{wr}}{\Theta}), \quad (25)$$

where ΔA_w denotes the area of the reflecting element under consideration, W represents the total number of reflective elements, ρ_w stands for the reflecting coefficient of the surface area ΔA_w, d_{tw} refers to the distance between T_x and the reflecting element, and d_{wr} represents the distance between the reflecting element and R_x. Similarly, the CIR of the non-line-of-sight (NLoS) component can be expressed as

$$h_{NLoS}(t) = \frac{A_p(m+1)}{2\pi}\sum_{q=1}^{Q}\frac{\Delta A_w \rho_m}{2\pi d_{tw}^2 d_{wr}^2}cos^m(\phi_{tw})cos(\theta_{tw}) \times cos(\phi_{wr})cos(\theta_{wr})T_s(\theta_{wr})g(\theta_{wr})rect(\frac{\theta_{wr}}{\Theta}) \times \delta\left(t-\frac{d_{tw}+d_{wr}}{c}\right). \quad (26)$$

TABLE 1. Agronomic greenhouse VLC system simulation parameters.

System model parameters	Values	References
Greenhouse scenario		
Dimensions (w $\times l \times h$)	(2 $\times$5 $\times$ 4)m	
Coordinates of the LEDs (x, y, z)	$T_1 = (-0.5, -1.25, 3.7)$, $T_2 = (0.5, 1.25, 3.7)$, $T_3 = (0.5, -1.25, 3.7)$, $T_4 = (-0.5, 1.25, 3.7)$	
Channel parameters		
Absolute temperature	295 K	[25], [29]
Background dark current	10 nA	[25], [29]
Boltzmann constant	1.38×10^{-23} J/K	[25], [29]
Capacitance	112×10^{-8} F	[25], [29]
Electronic charge	1.6×10^{-19} C	[25], [29]
FET channel noise factor	1.5	[25], [29]
FET transconductance	0.03 A/V^2	[25], [29]
Noise bandwidth	100 MHz	[25], [29]
Noise bandwidth factor I_2	0.562	[25], [29]
Noise bandwidth factor I_3	0.0868	[25], [29]
VLC transceiver parameters		
Average output optical power	10 W	[25], [29]
Band-pass filter of transmission	1	[25], [29]
Gain of the optical filter	1	[25], [29]
LED rotation angle	45°	[29]
LED tilt angle	45°	[29]
Modulation	on-off keying (OOK)	[25], [29]
Modulation bandwidth	50 MHz	[25], [29]
Modulation index	0.3	[25], [29]
Number of PDs	1	
PD physical area	1 cm^2	[25], [29]
Optical filter bandwidth	340 nm to 694.3 nm	[30]
Optical filter center wavelength	340 $\pm$2 nm	[30]
Optical filter full width half max	10 $\pm$2 nm	[30]
Refractive index	1.5	[25], [29]
Reflection coefficient	0.8	[25], [29]
Responsivity	0.53 A/W	[25], [29]
Rx FoV	60^o	[25], [29]
Tx semi-angle at half power	60^o	[25], [29]

VI. RESULTS AND ANALYSIS

A. ILLUMINANCE DISTRIBUTION IN THE GREENHOUSE ENVIRONMENT

This part is all about judging how well the VLC system works in an agronomic greenhouse setting using the channel we came up with in Section V. First, we analyze the illuminance conditions in the greenhouse scenario through simulations. Second, we analyze and simulate basic performance metrics for wireless communication systems in a greenhouse environment, such as CIR, received power, BER, and SNR. For simulation, we used a greenhouse with dimensions of 2 m x 5 m x 4 m. In our analysis, without losing generality, we consider four LEDs, with fixed rotation and tilt angles for ease, and a single PD. It should be emphasized that the LED positions are referential only to verify the feasibility of the proposed VLC channel model. We also considered inclusion in the simulation of molecular constituents and aerosols produced by snow or rain in the environment to demonstrate the effect on the performance metrics to be evaluated. All evaluations are numerical and created using simulations in Matlab software, applying the ray-tracing methodology for the optical links and Monte Carlo simulations. The most relevant parameters used for the development of the simulations, with their respective values and references, can be seen in Table 1.

As we mentioned at the beginning of our work, in addition to providing a robust and effective communication system in agronomic greenhouses, it is also proposed that VLC offers adequate lighting in these environments. Since LEDs are an artificial source of direct light, we initially presented a mathematical model to calculate the illuminance of LEDs. Therefore, to calculate this parameter, we define the luminous flux Q as the optical power that the human eye can receive in the following expression [13], [25]:

$$Q = 683 N_{T_x} \int_{380}^{720} S(\lambda) V(\lambda) d\lambda, \tag{27}$$

where $V(\lambda)$ is the sensitivity function of the human eye and $S(\lambda)$ is the distribution of the radiation spectrum. The relationship between Q and the illuminance $I(\phi)$ on the PD is given by [13], [25]

$$I(\phi) = \frac{\delta Q}{\delta A_p} = \sum_{j=1}^{N_{T_x}} j I_0 \cos^m(\phi), \tag{28}$$

where I_0 is the center of light intensity of T_x. This expression allows us to calculate the light intensity in the PD reception plane. However, we need baseline data on greenhouse illuminance to compare with our analysis. Consequently, the results are contrasted with the general rules established for illuminance in these scenarios. Among the minimum light intensity requirements for greenhouses, they must comply with a minimum illuminance of [70-100] *lux* [30]. Taking these values into account, we obtain the illumination in the agronomic greenhouse scenario, as shown in Fig. 6.

On the basis of Fig. 6, we can see that the illuminance values range from [600-900] lux. It is also observed that the highest illuminance values are found in the center of the greenhouse. This is due to the location of the LEDs in the scenario and their tilt and rotation. Precisely, the center of the greenhouse, where all the crops are located, must be the area with the greatest illuminance, first to keep the crops in an optimal condition and second to obtain the highest optical power that can reach the PD. When we compare the results with the minimum illuminance values in the standard, the illuminance standard for agronomic greenhouse environments is met [].

B. CHANNEL IMPULSE RESPONSE OF VLC SYSTEM IN A GREENHOUSE ENVIRONMENT

We showed the CIR at every point in the greenhouse to test the derived VLC channel model in agronomic greenhouse settings and make sure this method works as expected. The CIR, which we represent as $h_{greenhouse}(t)$ is defined as the optical intensity received when the transmitted optical intensity is a Dirac delta function of the unit area. Therefore, $h_{greenhouse}(t)$ can be obtained from the expression (17), adding the delta components $\delta(\cdot)$, which depends on the distance it travels the light beam, as follows:

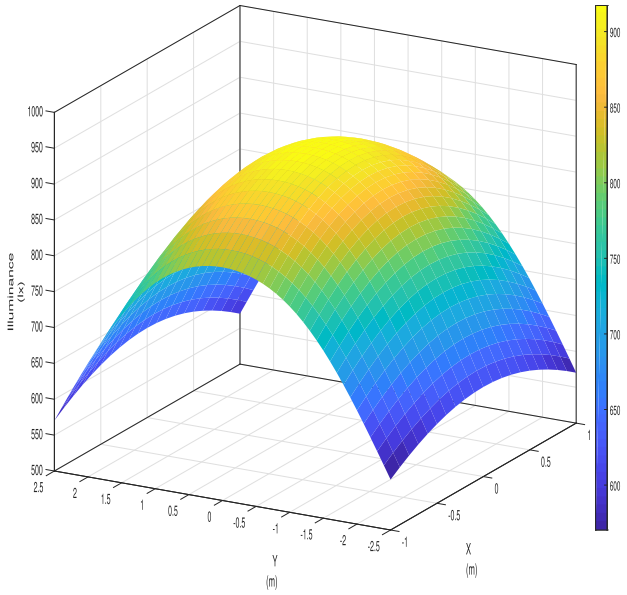

FIGURE 6. Illuminance distribution of greenhouse agronomic scenario.

$$h_{greenhouse}(t) = h_{LoS}(t)\delta\left(t - \frac{d_{ij}}{c}\right) + h_{NLoS}(t) \times \sum_{w=1}^{W} \delta\left(t - \frac{d_{iw} + d_{wj}}{c}\right). \tag{29}$$

Fig. 7 shows the distribution of CIR throughout the simulated greenhouse environment. The number of partitions is set to 18 for X and Y and to 15 for Z. The spatial resolution is set to 0.33 m for X and Z, and 0.16 m for Y. The temporal resolution is set to 0.25 ns. In the graphic several interesting findings can be distinguished. First, we can notice that the CIR in the complete scenario varies between a range of values of $[0.8\times10^{-7} - 8.1 \times 10^{-7}]$. Second, in terms of the theoretical aspect, as the distance between the LEDs and the PD increases, the CIR magnitude should decrease. However, this does not occur in the agronomic greenhouse scenario. If we observe the distribution of Fig. 7, we note that the CIR is not uniform and that its decrease is not inversely proportional to the distance between the LEDs and the PD. This effect is due to the position of the LEDs and their angles of inclination and rotation. This causes the largest magnitude values of the CIR to be in the center of the stage. We also observed a drop in CIR magnitudes in certain parts of the greenhouse. This is due to the higher concentration of constituent molecules and aerosols, which affects the optical paths because they absorb or reflect light, producing a vertiginous decrease in the CIR.

If we compare the CIR values obtained in this work with the CIR values obtained in other environments, such as [29], we may notice some differences. The CIR values obtained in the greenhouse are lower than those obtained for underground mines and much lower than those obtained for ideal indoor VLC environments. This comparison gives us an idea that the greenhouse's external environment is difficult to control and

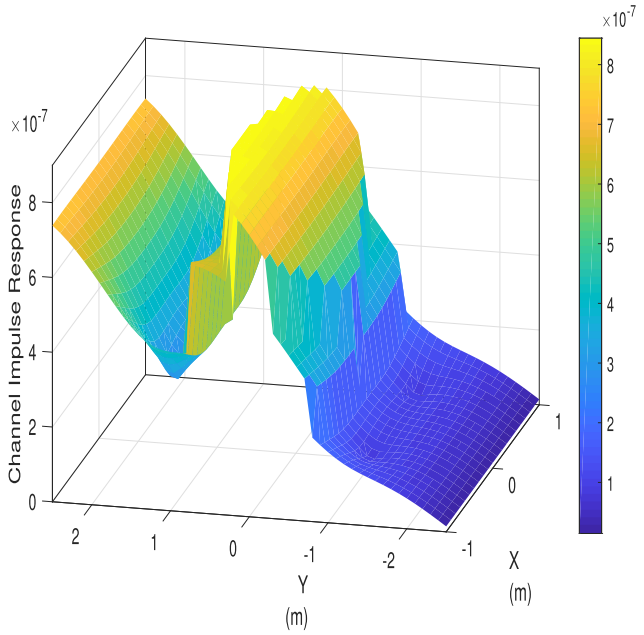

FIGURE 7. CIR distribution of greenhouse agronomic scenario.

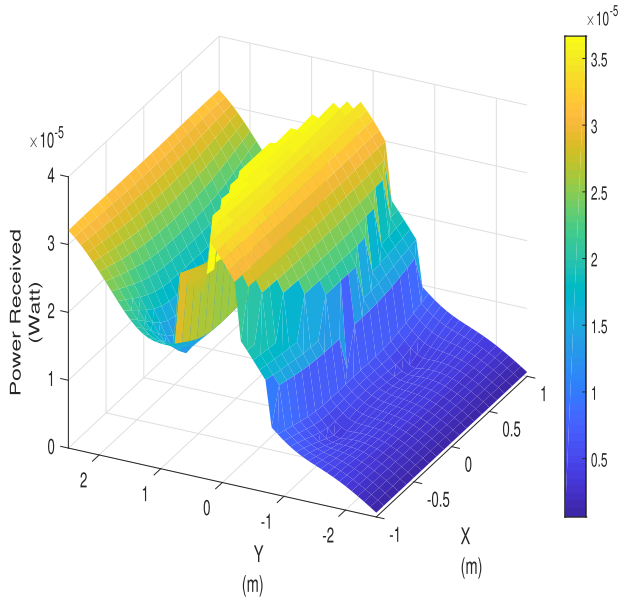

FIGURE 8. Distribution of the power received in the greenhouse agronomic scenario.

that its atmospheric variables produce a harmful effect on the optical links.

C. POWER RECEIVED OF VLC SYSTEM IN A GREENHOUSE ENVIRONMENT

Because we only consider one PD and four LEDs in our proposed agronomic greenhouse scenario, we use the expression from equation (20) to find out how much power the PD gets from the light of the LEDs.

Fig. 8 shows the graphical distribution of the power received in the evaluated agronomic greenhouse scenario. The power received in the complete scenario varies between a range of values of $[0.82\times10^{-5} - 3.8 \times 10^{-5}]$ W. Let us compare these power values with underground mining VLC scenarios or ideal indoor VLC scenarios [29]. We can see that the powers received in the proposed greenhouse environment are lower. Furthermore, the power distribution obtained is not uniform and is not always directly proportional to the distance between the LEDs and the PD. Therefore, we observe that the effect of the rotation and tilt of the LEDs and the atmospheric factors of the environment that produce aerosol particles and constituent molecules influence the received optical power levels.

Finally, we can see that the received power distribution that we obtain follows the same pattern as the CIR, so we can deduce that our results are consistent.

D. SIGNAL-TO-NOISE-RATIO OF VLC SYSTEM IN A GREENHOUSE ENVIRONMENT

In the proposed VLC system designed for agronomic greenhouses, employing intensity modulations with IM/DD is essential. In our study, OOK modulation has been utilized. To facilitate reliable communication, it is crucial to calculate the SNR, which sets the groundwork for ensuring an optimal Bit Error Rate (BER) in the subsequent subsection. The methodology for calculating the SNR in our research is derived from the expression outlined in [13], [25]:

$$SNR = \frac{rP_r}{\sigma^2_{total}}. \tag{30}$$

Fig. 30 illustrates the SNR across the entire coverage area of the greenhouse under rainy conditions, which result in the presence of aerosols and constituent molecules within the greenhouse. The SNR across this complete scenario ranges between [3.25-39.32] dB. This graph shows that the SNR distribution in the greenhouse is similar to the wavy pattern seen in the Channel Impulse Response (CIR) and received power. Notably, the highest SNR values are not located at the center of the greenhouse, an effect primarily attributed to the heightened presence of noise factors (such as thermal and shot noise) in the central region. Additionally, the distribution of aerosols and constituent molecules within the greenhouse is random, leading to lower SNR values in certain areas, especially when weather conditions intensify. This results in greater attenuation, absorption, and dispersion of the signal, which in turn is more significantly affected by noise.

Finally, we can observe that we have positive SNR values throughout the greenhouse scenario, so we can affirm that there is coverage of the optical signal throughout the analyzed environment.

E. CHANNEL IMPULSE RESPONSE OF VLC SYSTEM IN AN UNDERGROUND ENVIRONMENT

In this section, we will thoroughly analyze the behavior of the UM-VLC channel and evaluate the performance of the UM-VLC system. We will achieve this through the use of powerful computational simulations developed in Matlab. The evaluation metrics used will be the CIR, received optical

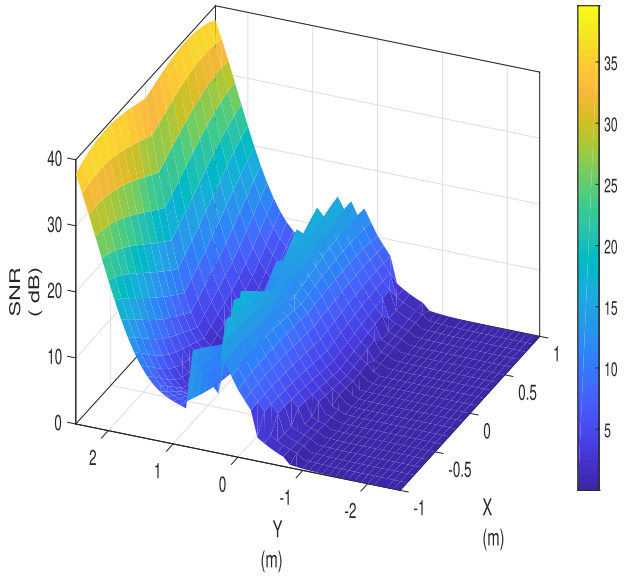

FIGURE 9. SNR distribution of greenhouse agronomic scenario.

TABLE 2. UM-VLC system simulation parameters.

System Model Parameters	Values	References
UM scenario parameters		
Coordinates of the T_x (x, y, z)	$(1 \times 5 \times 3.5)$ m	
Dimensions of the tunnel $(w \times l \times h)$	$(2 \times 10 \times 3.7)$ m	
Wall reflection coefficient	0.8	[27], [28]
Wall rotation angle	$U[0,180°]$	[27], [28]
Wall tilt angle	$U[0,180°]$	[27], [28]
VLC transceiver parameters		
Average output optical power	10 W	[27], [28]
Gain of the transmission band-pass filter	Unity Gain	[27], [28]
Gain of the optical filter	Unity Gain	[27], [28]
Helmet position (miner's height)	1.7 m	
Number of R_x	1	
PD physical area	1 cm^2	[27], [28]
Refractive index	1.5	[27], [28]
Responsivity	0.53 A/W	[27], [28]
R_x FOV	60°	[27], [28]
R_x rotation angle	45°	[27], [28]
R_x tilt angle	45°	[27], [28]
T_x semi-angle at half power	60°	[27], [28]
T_x rotation angle	45°	[27], [28]
T_x tilt angle	45°	[27], [28]
General Parameters		
Estimation sequence length	24 bits	[31]
Modulation Scheme	OOK	[31]
Frame length	24717 bits	[31]
Number of frames	122	[31]
Optical watch	200 KHz	[31]
Sampling rate	2 samples/bit	[31]
Transmission rate	100 Kbps	[31]

power, and BER. We have meticulously selected the most relevant parameters for the development of these simulations, along with their respective values and references, which can be found in Table 2.

In order to determine the CIR, we took into account the parameters listed in Table 2. Additionally, we introduced two different scenarios for mobile obstructions entering the tunnel. The first scenario follows a Poisson distribution with an intensity parameter ϵ of five arrivals per minute [27]. The second scenario follows a Gaussian Bi-modal model. Fig. 10 displays the CIR graphs for each point in both simulated scenarios. milímetro.

Fig. 10(a) illustrates the CIR in the presence of mobile obstructions, which are modeled using a Poisson process. The curve reaches a maximum value of 5.43×10^{-7}, with a 95% confidence interval ranging from 5.15×10^{-7} to 5.70×10^{-7}. On the other hand, the minimum value is 0.28×10^{-7}, with a 95% confidence interval between 0.266×10^{-7} and 0.294×10^{-7}. The yellow regions in Fig. 10(a) are closer to T_x, resulting in a shorter distance between T_x and R_x. As a result, these regions exhibit higher CIR values compared to other parts of the scenario. On the contrary, the blue regions are farthest from T_x, leading to lower CIR values. The central area of the UM scenario demonstrates shadowing effects, where objects obstruct the LoS component of the VLC channel. Consequently, this area exhibits the lowest CIR values in the entire scenario.

Fig. 10(b) illustrates the CIR under the influence of mobile obstructions, following the Gaussian Bi-modal model. The curve reaches a maximum value of 6.89×10^{-7}, with a 95% confidence interval ranging from 6.55×10^{-7} to 7.23×10^{-7}. Conversely, the minimum value attained is 1.01×10^{-7}, with a 95% confidence interval between 0.96×10^{-7} and 1.06×10^{-7}. A comparison between Figs. 10(a) and 10(b) reveals several distinctions. Firstly, the CIR experiences a consistent decline in the scenario with the Gaussian bimodal model. Due to the shadowing that mining workers cause on VLC links, this decline occurs. In most cases, the dimensions of these obstructions do not completely block the components of the VLC channel, which is not the case with mobile machinery.

In both scenarios, the impact of NLoS and scattering elements is also evident. Although the optical signal is completely obstructed at specific time intervals, its amplitude never reaches zero. Reflective surfaces such as dust particles and walls cause the optical signal to interact with them, resulting in a lower intensity when it reaches R_x.

F. POWER RECEIVED OF VLC SYSTEM IN AN UNDERGROUND ENVIRONMENT

Fig. 1(a) illustrates the power distribution received in the simulated UM scenario using the Poisson process for obstructions. The maximum received power is −18.45 dBm, with a confidence interval 95% ranging from −19.37 dBm to −17.53 dBm. On the other hand, the minimum received power is −44.96 dBm, with a 95% confidence interval between −47.20 dBm and −42.71 dBm. It is evident that the received power distribution is non-uniform and does not always exhibit a direct proportionality with the distance between T_x and R_x. Moreover, there is significant variability in power values, even between closely located points in the scenario. This variability can be attributed to factors such as the orientation of T_x and R_x, signal reflection on non-flat walls, and shadowing. It should be noted that all areas in the UM scenario have some power value, indicating complete system coverage across the surface.

On the contrary, the received optical power distribution in the simulated UM scenario using the Gaussian bimodal model for obstructions is shown in Fig. 11(b). The maximum received power is −15.2 dBm, with a confidence interval 95%

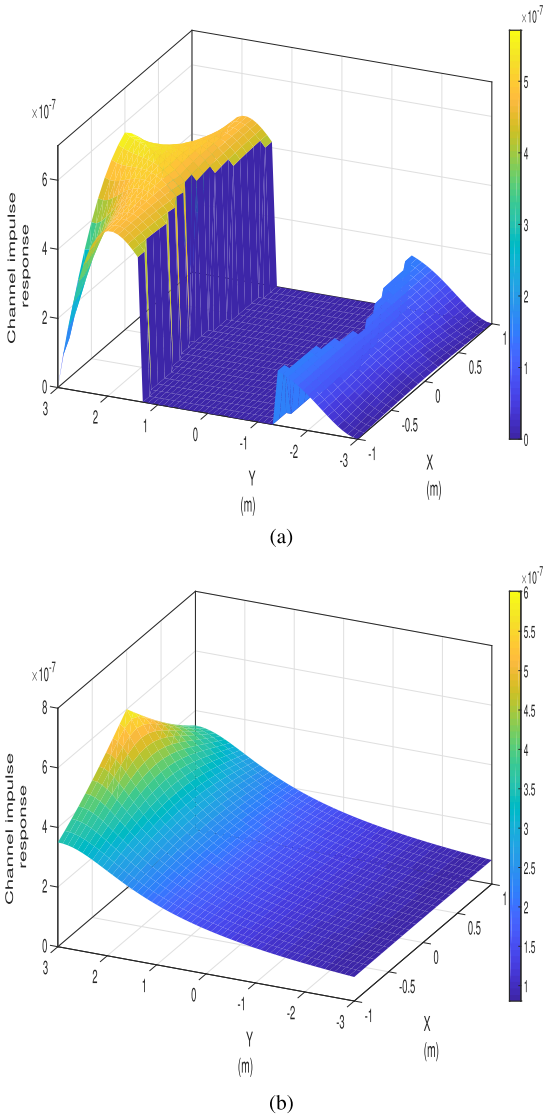

FIGURE 10. CIR considering mobile obstructions that follow a (a) Poisson process and (b) Gaussian Bi-modal model.

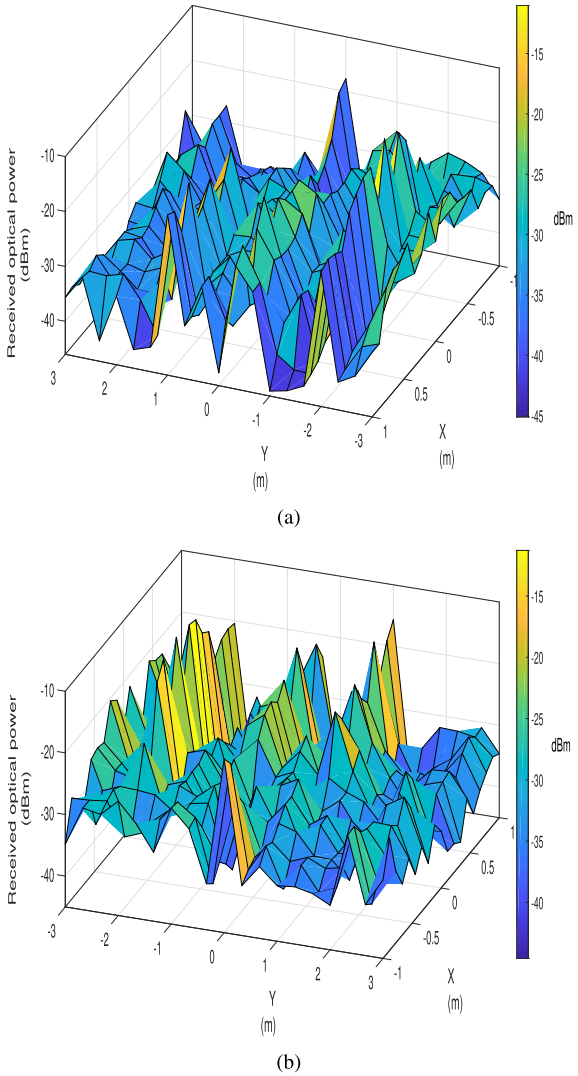

FIGURE 11. Received optical power considering mobile obstructions that follow a (a) Poisson process and (b) Gaussian Bi-modal model.

ranging from −15.96 dBm to −14.44 dBm. The minimum received power is −40.16 dBm, with a confidence interval 95% between −42.16 dBm and −38.16 dBm. Similarly to the distribution shown in Fig. 11(a), the power distribution in Fig. 11(b) also exhibits nonuniformity and high variability. However, the variability of power values is lower when using the Bi-modal Gaussian model.

G. SENSORS PROPOSAL FOR GREENHOUSE APPLICATIONS

After conducting a detailed review of the sensors available at the monitoring station, it has been concluded that it is necessary to update the hardware used for data collection with sensors that are more suitable for use in the agricultural field.

The hardware upgrade will improve the accuracy and reliability of the collected data, which is essential to ensure proper decision-making in agricultural management. Additionally, the use of more advanced sensors will allow more detailed information on environmental and soil conditions, which can be of great use in optimizing agricultural processes. For this reason, a proposal for new sensors has been developed and shown in Table 3.

Sensors selected in Table 3 for hardware upgrade have a higher IP protection rating compared to sensors previously used at the monitoring station. In addition, most of these sensors operate on the same communication protocol, Modbus, making the system more scalable in the long run.

The higher IP protection rating means that the sensors are more resistant to dust and water, increasing their durability and reliability in agricultural environments where conditions can be more challenging. Furthermore, the use of the modBus protocol will allow greater compatibility and integration capabilities with other devices and systems in the future, making the system more scalable and adaptable to changing needs.

Compared to classic Arduino sensors, Modbus sensors offer several advantages. Firstly, Modbus sensors are more

TABLE 3. New sensor proposal.

Variable	Sensors
Temperature	PR 3002 GZWS NO 1
Humidity	PR 3002 GZWS NO 1
Solar Radiation	PR-300AL-UV-N01
Wind speed transmitter	PR-3000-FSJT-N01 or APRS weather kit
Wind direction sensor	PR-3000-FXJT-N01 or APRS weather kit APRS Weather kit
Ph	PR-3000-TR-PH
Humidity	PR-3000-ECTH-N01 or APRS weather kit
Rain Sensor	PR-3001-GYL-N01 or APRS Weather Kit APRS Weather Kit

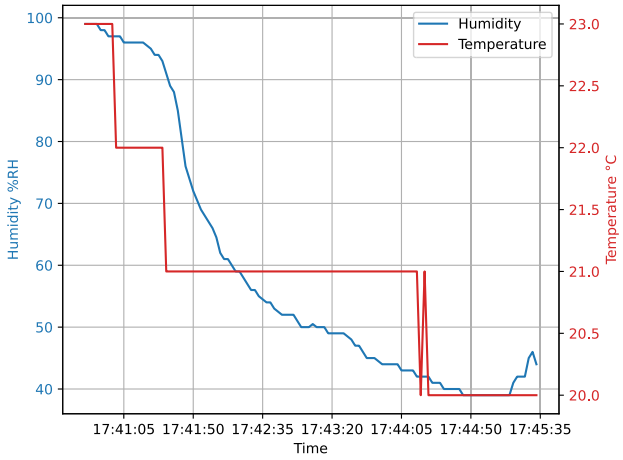

FIGURE 12. Temperature and humidity obtained of sensor DHT22.

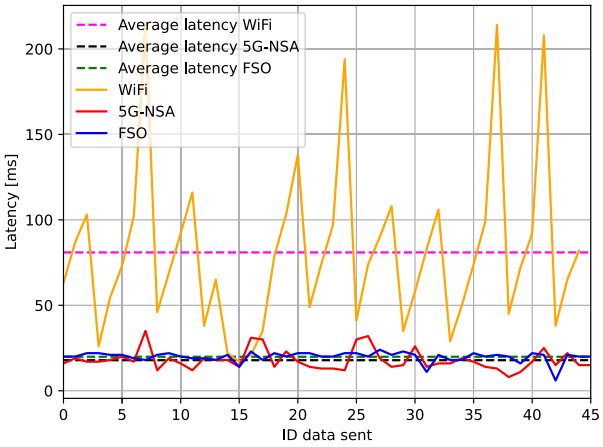

FIGURE 13. Wi-Fi vs 5G vs FSO latency.

accurate and reliable as they are designed for industrial and automation applications. Additionally, Modbus sensors can be easily integrated into existing control and monitoring systems, making them ideal for IoT projects that require the integration of multiple systems and devices.

Another advantage of Modbus sensors is that they offer higher data transmission speeds and wider diagnostic capabilities than classic Arduino sensors, allowing for more efficient and precise monitoring. In summary, Modbus sensors are an ideal choice for IoT projects that require high reliability, precision, and scalability.

H. SENSOR TEMPERATURE AND HUMIDITY MEASUREMENTS

The present experiment is executed using a *Python* script that retrieves humidity and temperature data from a DHT-22 sensor through serial communication. The functionality of Telegraf-based server communication is evaluated. This examination uses code written in the programming language *Python*; this code is tasked with transmitting the data.

It is crucial to define the data frame that will be utilized, as this determines not only the graphics that will be exhibited in user applications but also the data set that will be graphed locally on the server.

Fig. 12 corresponds to the temperature and humidity measurements during a time interval of five minutes. In the graph, the y-axis is dimensionless because it represents two variables with different units of medication.

I. LATENCY MEASUREMENTS FOR SEVERAL TECHNOLOGIES

To evaluate the uplink and downlink times and distributions of the hybrid twin with UM-VLC and the greenhouse channels, three data transmission tests were performed to reach the control center. Normally, FSO is used for uplink and downlink because it is necessary to read the sensors and act on the motors in the tunnel and greenhouse. On the other hand, 5G-NSA is used to reach a control center far from the tunnel and the greenhouse. WIFI is used to have an alternative path to the wiring in the control center.

Fig. 13 indicates that the average latency value for WiFi is 81 ms and for 5G is 18 ms. Therefore, when 5G is compared to Wi-Fi, there is a 78% reduction in latency. The average latency of the FSO link can be shown to be 20 ms, which is just 2 ms higher than what was achieved in the 5G network.

J. LATENCY DISTRIBUTION FOR SEVERAL TECHNOLOGIES

It is a common misconception among telecom engineers that a WiFi network developed for an indoor environment will work in an underground tunnel. However, empirical evidence suggests that this is not the case. The tunnel acts as a waveguide and alters transmission and reception. On the other hand, WiFi works well as an urban channel in a greenhouse and represents an opportunity for diversity with VLC and radio.

The density function depicted in Fig. 14 outlines the spread of latency for data transmitted within the predefined time interval. For Wi-Fi, it's observed that the bulk of latency values predominantly cluster within the ranges of 50 to

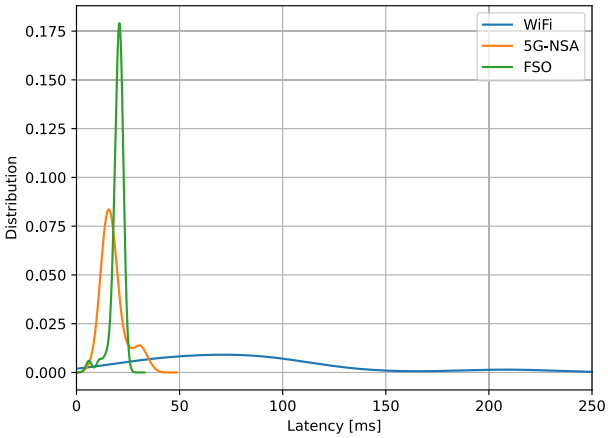

FIGURE 14. Wi-Fi vs 5G vs FSO latency distribution.

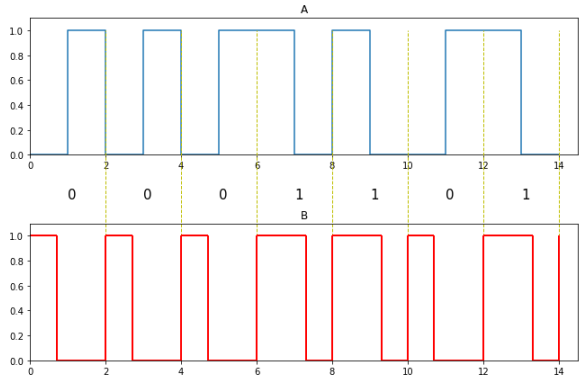

FIGURE 15. Comparison between standard manchester modulation and the proposed manchester modulation.

100 ms and 200 to 250 ms. In contrast, with 5G, a multinormal distribution tends to concentrate around a singular value, not exhibiting the range of values seen with Wi-Fi. When compared to the Free Space Optics (FSO) link, it's evident that its distribution is significantly more focused around a single value of 20 ms, showcasing a narrower dispersion relative to the aforementioned technologies [32].

K. BIT ERROR RATE CURVES FOR GREENHOUSE AND UNDERGROUND ENVIRONMENTS

In this work, On-Off Keying (OOK) modulation is utilized. This modulation facilitates the representation of two states: the LOW logical value, which signifies a zero, and the HIGH logical value that signifies a 1, via the application of Manchester Encoding. Manchester Encoding is a communication system employed in conjunction with OOK modulation, wherein a transition between two signal levels occurs at each logical bit time.

In Fig. 15, a detailed comparison is illustrated between conventional modulation and the Manchester modulation technique. This approach requires the use of two physical bits for the transmission of every logical bit. The primary difference from the traditional Manchester encoding method lies in the temporal length of each signal state. Specifically, to denote a logical 0, one-third of the duration for the two physical bits is assigned to the high state, with the balance

FIGURE 16. Underground tunnel under extreme dust conditions.

spent in the low state. Conversely, to signify logical 1, although the sequence of high and low states remains unchanged, the high state now extends over two-thirds of the total duration for the two physical bits, with the remainder in the low state. This refined modulation strategy obviates the necessity for clock synchronization between the transmitting and receiving entities, thereby simplifying the communication process.

The equations 15, 16, 24, and 26 can be implemented in various ways depending on the available transmitter-receiver pair. For example, a LED and a photodetector, an infrared laser LED and a photodiode, or an infrared laser LED with a photoresistor, depending on the costs and the desired reach. For instance, an LED and a photodetector achieve only a few centimeters and are mostly used in demonstrations, whereas an infrared laser LED with a photodiode or photoresistor are better focused and have a greater range.

Fig. 16 shows the experiment carried out in an underground tunnel under severe dust conditions, to validate the mathematical model by using a two-dimensional disc for particle distribution. This approach aligns with Equations 24 and 26, which encapsulate the model detailed in [29]. Table 2 elaborates on the simulation parameters, which are suitable for any type of LED across a comprehensive wavelength spectrum extending from 400 to 700 nm. In this particular experiment, a white LED and a photodiode were used, the same as those used in greenhouse applications for a fair comparison, achieving distances of up to 8 meters with ease. For further extending the reach, Infrared Light-Emitting Diodes (IR LEDs) can be utilized. These diodes are adept at emitting infrared radiation at the boundary of the visible light spectrum and are expressly designed for the infrared spectrum, typically covering the range from 700 nm to 1 mm.

Fig. 17 shows a BER comparison between UM-VLC and greenhouse VLC systems. Three curves are presented for each scenario. The black curves represent the ideal AWGN simulation without large disturbances in both the underground and greenhouse environments, whereas the green curves represent both environments simulated under the theoretical parameters addressed in this article. Finally, the blue curves represent the BER obtained experimentally in both scenarios, under the technical parameters described in this section.

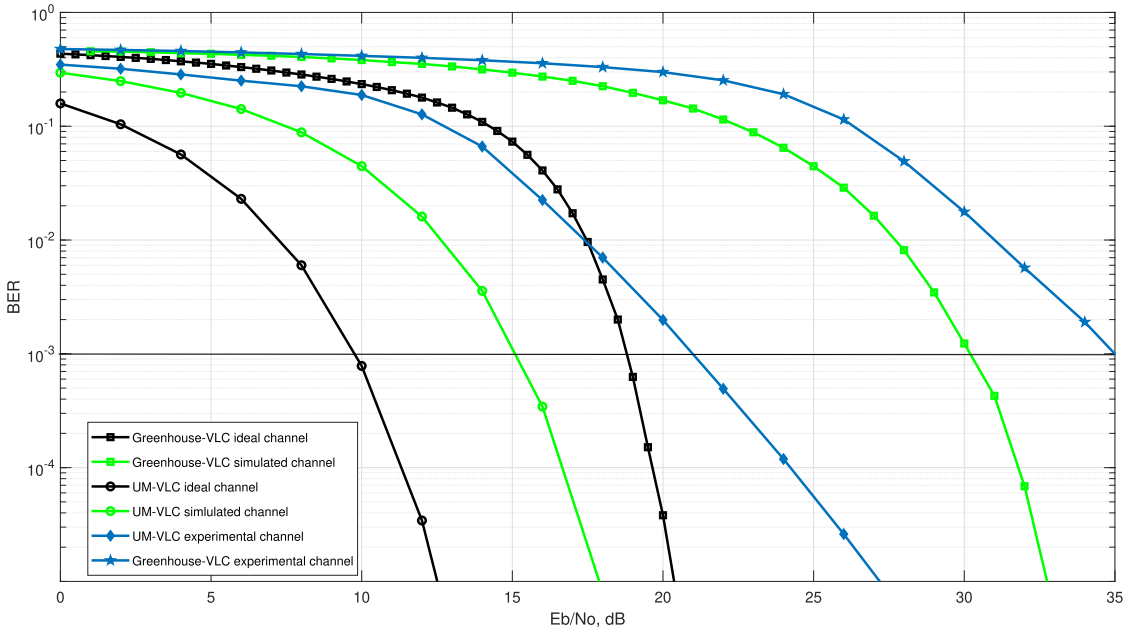

FIGURE 17. BER comparison between UM-VLC and greenhouse VLC systems.

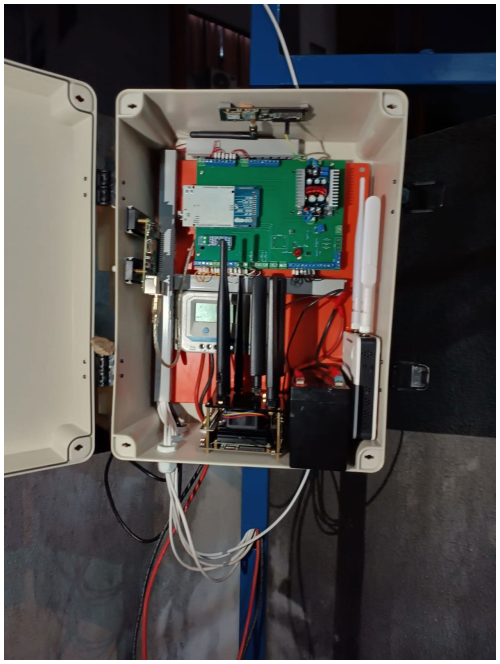

FIGURE 18. Concentratue with Wi-Fi vs 5G vs FSO latency distribution.

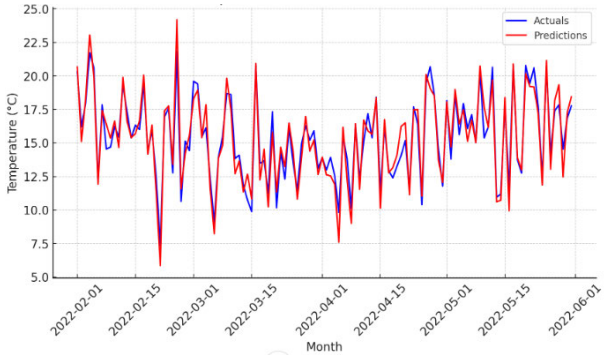

FIGURE 19. Temperature prediction.

The significant discrepancy in the BER curves between the ideal, simulated and experimental scenarios in Fig. 17 highlights the challenges in achieving real-world performance that closely aligns with theoretical expectations in VLC systems. This disparity can be attributed to various factors, such as real environmental conditions that can affect signal transmission, limitations in the practical implementation of theoretical parameters, and interference not considered in the simulated models. Furthermore, variability in the received power distribution and lack of proportionality with the distance between the LEDs and the PDs or optical receivers may also contribute to this discrepancy. In fact, the BER curves obtained in completely controlled ideal environments, seen in Fig. 17, help us to notice how the environment affects the performance of the VLC systems, since the BER degrades if we compare it with the simulated or experimental curves.

On the other hand, research on wireless optical communication systems highlights the importance of analyzing signal behavior and propagation models in detail to fully evaluate communication systems in greenhouse and underground environments. In context, the differences in the BER curves between the ideal, simulated, and experimental scenarios highlight the complexity of translating theory into practice in VLC systems and underline the importance of considering real-world conditions and propagation models to achieve optimal performance in harsh environments.

In more detail, if we draw a line at 10^{-3}, the gain between the simulated miner channel and the simulated greenhouse channel shows a gain of almost 10 dB at a distance of 4 meters.

Keeping the line at 10^{-3}, the gain between the simulated miner channel and the experimental one is 6 dB at a distance of 4 meters and 8 dB for a distance of 8 meters.

In the case of the greenhouse, if we draw a line at 10^{-3}, the gain between the simulated greenhouse channel for a distance of 4 meters is 13 dB and 17 dB for a distance of 8 meters.

L. ANTENNA DESIGNED FOR DATA COLLECTION IN BOTH GREENHOUSE AND UNDERGROUND ENVIRONMENTS

In the preceding section, we evaluated the performance of various models, focusing on their BER. Fig. 18 illustrates the concentrator equipment used to collect data from the greenhouse and the tunnel. This setup is capable of receiving demodulated light signals and transmitting the data to the DT using a variety of technologies, as outlined in the mathematical models discussed in Sections V and IV. The equipment array includes a Wi-Fi antenna, a 5G antenna with multiple elements, and an FSO subsystem, which is not shown here. We used this configuration to conduct experimental measurements, the results of which are presented in Fig. 14. This figure offers a comparative analysis of Wi-Fi, 5G, and FSO technologies in terms of latency and connectivity performance.

M. TEMPERATURE PREDICTION

Creating a robust training data set is crucial in developing an LSTM model, which is intended for anomaly detection in temperature control systems. This meticulous process starts with careful feature selection, identifying those critical factors based on domain knowledge and analysis of the system's physical behavior. The information is structured into temporal sequences that fit the format required by the LSTM models, where each time segment constitutes an independent sample that contributes to pattern learning. Keras is used, a Deep Learning library that is part of the TensorFlow ecosystem, optimized for sequential data processing and particularly suitable for interpreting the complexity associated with temperature data.

During the LSTM model training phase, libraries such as pandas, numpy, matplotlib.pyplot, and seaborn are essential for data management. At the same time, tools from Keras such as `keras.preprocessing.sequence` and `TimeSeriesGenerator` provide the necessary infrastructure for efficient data preparation. Adjusting the weights and biases through optimization algorithms, such as gradient descent, the model accurately minimizes the difference between the predictions and the actual data. This process not only enables the model to predict the temperature, but also makes it insightful in identifying patterns indicative of contingencies.

The process concludes with a detailed evaluation, comparing the predictive performance of the model with a test data set. For example, Fig. 19 represents the actual measurements from a temperature sensor connected to the board and the temperature predictions. To evaluate the model, the best model of the elapsed epochs is loaded, and predictions are made using the method based on the data of the training and test set. A one-day lag adjustment is made to the theoretical lag of the model, and then a data frame is created to store the predictions along with the actual output. This evaluation resulted in a mean squared error of 0.5405, reflecting the correspondence between predictions and actual values throughout the first half of 2022. This allows a more graphical visualization and comparison of the data, in accordance with the mathematical concepts discussed in the previous sections.

VII. CONCLUSION

In this article, we present a cutting-edge hybrid twin model designed to simulate and improve the operational efficiency of greenhouse and underground environments. This is achieved through the innovative application of radio communication technologies, such as LoRa, alongside free-space optical channels, including VLC and FSO. Our goal is to pave the way for the creation of advanced, reliable, and robust agricultural products, thus advancing the capabilities of smart agriculture.

In the future, with the application of suitable actuators, greenhouses can be darkened to mimic an underground tunnel environment. Consequently, it becomes essential to have a DT that enables the evaluation and comparison of light effects on a communication channel. This need arises from the unique characteristics specific to greenhouse settings. Furthermore, when evaluating lighting conditions within the greenhouse, it is found that the illumination delivered by the VLC system aligns with international benchmarks for such environments, exhibiting light intensity levels that range from 600 to 900 lux.

Concerning the received power and the CIR, it is evident that their distributions are asymmetrical and their magnitudes are diminished in comparison to alternative interior scenarios. The magnitudes of the LoS and non-LoS components change, spread out, and weaken because of things in the environment and the orientation effects of the LEDs.

Finally, the SNR for our proposed greenhouse scenario has been detailed. Defining a threshold at 10^{-3}, we observe that the gain difference between the simulated miner channel and the simulated greenhouse channel approaches nearly 10 dB at a distance of four meters. Maintaining this threshold, the comparison reveals a gain of 6 dB at a four-meter distance and 8 dB at an eight-meter distance between the simulated miner channel and the experimental setups. Specifically for the greenhouse scenario, setting the reference at 10^{-3} allows us to note that the gain for the simulated greenhouse channel reaches 13 dB at a distance of four meters, illustrating the effectiveness of our proposed modifications in improving signal quality over various distances.

We developed a VLC channel model for UM that accounts for five key physical and environmental factors that impact the optical signal: LED and PD orientation, wall irregularities, shadowing, and dust scattering. To quantify the shadowing effect induced by mobile machinery and agricultural workers within the tunnel, we employed two

statistical approaches: the Poisson process and the bi-modal Gaussian model. These models were integrated into the analytical framework of the UM-VLC channel model, although with limited detail, as they have been explored in our previous research. Using DTs, we can quickly gather field data and compare it with computer simulations to deduce the CIR and the distribution of received optical power for the UM-VLC system. Our study highlights the dominant impact of shadowing, as compared to dust scattering, on the efficacy of optical communications. Specifically, mobile machinery presents a considerable threat by potentially obstructing communication links entirely in certain tunnel sections. This finding reveals a notable superiority of underground environments over greenhouse settings in all scenarios examined.

The concept of a hybrid DT stands out by significantly enhancing the precision of simulations and minimizing errors to nearly negligible levels. This breakthrough allows for the analysis of large-scale systems or complex systems of systems, an endeavor that would be exceedingly challenging with traditional physics-based simulation models alone. DTs emerge as a formidable solution to transition existing systems toward smarter and more integrated frameworks capable of addressing a wide array of challenges, from labor and environmental issues to production inefficiencies. However, despite their potential, the full capabilities of DTs in precision agriculture remain largely unexplored. Any effort toward bridging these concepts could greatly accelerate their integration into an infrastructure that seamlessly combines various IT systems, marking a pivotal step in realizing the vast benefits of digital transformation in agriculture.

REFERENCES

[1] M. Shang, G. Tian, L. Qin, J. Zhao, H. Ruan, and F. Wang, "Greenhouse wireless monitoring system based on the ZigBee," in *Proc. Int. Conf. Comput. Comput. Technol. Agriculture*, 2013, pp. 109–117, doi: 10.1007/978-3-642-36124-1_14.

[2] C. Verdouw, B. Tekinerdogan, A. Beulens, and S. Wolfert, "Digital twins in smart farming," *Agricult. Syst.*, vol. 189, Apr. 2021, Art. no. 103046. [Online]. Available: https://linkinghub.elsevier.com/retrieve/pii/S0308521X20309070

[3] N. Ariesen-Verschuur, C. Verdouw, and B. Tekinerdogan, "Digital twins in greenhouse horticulture: A review," *Comput. Electron. Agricult.*, vol. 199, Aug. 2022, Art. no. 107183. [Online]. Available: https://linkinghub.elsevier.com/retrieve/pii/S0168169922005002

[4] M. Jans-Singh, K. Leeming, R. Choudhary, and M. Girolami, "Digital twin of an urban-integrated hydroponic farm," *Data-Centric Eng.*, vol. 1, p. e20, Dec. 2020. [Online]. Available: https://www.cambridge.org/core/product/identifier/S2632673620000210/type/journal_article

[5] N. Slob and W. Hurst, "Digital twins and Industry 4.0 technologies for agricultural greenhouses," *Smart Cities*, vol. 5, no. 3, pp. 1179–1192, Sep. 2022. [Online]. Available: https://www.mdpi.com/2624-6511/5/3/59

[6] T. I. Zohdi, "A digital-twin and machine-learning framework for the design of multiobjective agrophotovoltaic solar farms," *Comput. Mech.*, vol. 68, no. 2, pp. 357–370, Aug. 2021, doi: 10.1007/s00466-021-02035-z.

[7] M. S. Ahamed, M. Sultan, D. Monfet, M. S. Rahman, Y. Zhang, A. Zahid, M. Bilal, T. M. A. Ahsan, and Y. Achour, "A critical review on efficient thermal environment controls in indoor vertical farming," *J. Cleaner Prod.*, vol. 425, Nov. 2023, Art. no. 138923. [Online]. Available: https://linkinghub.elsevier.com/retrieve/pii/S0959652623030810

[8] M. P. Aher, S. M. Nikam, R. S. Parbat, and V. S. Chandre, "A hybrid wired/wireless infrastructure networking for green house management," in *Proc. Int. Conf. Autom. Control Dyn. Optim. Techn. (ICACDOT)*, Sep. 2016, pp. 1152–1157. [Online]. Available: http://ieeexplore.ieee.org/document/7877767/

[9] Y. S. Chang, Y. Hsiung Chen, and S. K. Zhou, "A smart lighting system for greenhouses based on narrowband-IoT communication," in *Proc. 13th Int. Microsystems, Packag., Assem. Circuits Technol. Conf. (IMPACT)*, Oct. 2018, pp. 275–278. [Online]. Available: https://ieeexplore.ieee.org/document/8625804/

[10] A. Mittal, N. N. Sarma, A. Sriram, T. Roy, and S. Adhikari, "Advanced agriculture system using GSM technology," in *Proc. Int. Conf. Commun. Signal Process. (ICCSP)*, Apr. 2018, pp. 285–289. [Online]. Available: https://ieeexplore.ieee.org/document/8524538/

[11] R. Sotner, J. Jerabek, L. Polak, J. Petrzela, W. Jaikla, and S. Tuntrakool, "Illuminance sensing in agriculture applications based on infra-red short-range compact transmitter using 0.35 μm CMOS active device," *IEEE Access*, vol. 8, pp. 18149–18161, 2020.

[12] X. Geng, Q. Zhang, Q. Wei, T. Zhang, Y. Cai, Y. Liang, and X. Sun, "A mobile greenhouse environment monitoring system based on the Internet of Things," *IEEE Access*, vol. 7, pp. 135832–135844, 2019.

[13] Z. Ghassemlooy, W. Popoola, and S. Rajbhandari, *Optical Wireless Communications*, 2nd ed. Boca Raton, FL, USA: CRC Press, 2018.

[14] N. Saeed, M.-S. Alouini, and T. Y. Al-Naffouri, "Toward the Internet of Underground Things: A systematic survey," *IEEE Commun. Surveys Tuts.*, vol. 21, no. 4, pp. 3443–3466, 4th Quart., 2019. [Online]. Available: https://ieeexplore.ieee.org/document/8793165/

[15] M. C. Vuran, A. Salam, R. Wong, and S. Irmak, "Internet of Underground Things in precision agriculture: Architecture and technology aspects," *Ad Hoc Netw.*, vol. 81, pp. 160–173, Dec. 2018. [Online]. Available: https://linkinghub.elsevier.com/retrieve/pii/S1570870518305067

[16] H. Esmaiel, H. A. Leftah, N. U. R. Junejo, and H. Sun, "Deep learning-based index modulation for underground communications," *IEEE Open J. Commun. Soc.*, vol. 4, pp. 2122–2132, 2023. [Online]. Available: https://ieeexplore.ieee.org/document/10238846/

[17] Y. Zhong and J. J. Tao, "Bio-inspired vibrational wireless underground communication system," *J. Rock Mech. Geotechnical Eng.*, vol. 14, no. 4, pp. 1042–1051, 2022. [Online]. Available: https://ieeexplore.ieee.org/document/10238846/

[18] A. Salam, M. C. Vuran, X. Dong, C. Argyropoulos, and S. Irmak, "A theoretical model of underground dipole antennas for communications in Internet of Underground Things," *IEEE Trans. Antennas Propag.*, vol. 67, no. 6, pp. 3996–4009, Jun. 2019. [Online]. Available: https://ieeexplore.ieee.org/document/8657723/

[19] M. Bertocco, S. Parrino, G. Peruzzi, and A. Pozzebon, "Estimating volumetric water content in soil for IoUT contexts by exploiting RSSI-based augmented sensors via machine learning," *Sensors*, vol. 23, no. 4, p. 2033, Feb. 2023. [Online]. Available: https://www.mdpi.com/1424-8220/23/4/2033

[20] M. Skiljo, Z. Blaževic, L. Dujic-Rodic, T. Perkovic, and P. Solic, "Self-sensing antenna for soil moisture: Beacon approach," *Sensors*, vol. 22, no. 24, p. 9863, Dec. 2022. [Online]. Available: https://www.mdpi.com/1424-8220/22/24/9863

[21] I. Palama, F. Gringoli, G. Bianchi, and N. Blefari-Melazzi, "IMSI catchers in the wild: A real world 4G/5G assessment," *Comput. Netw.*, vol. 194, Jul. 2021, Art. no. 108137. [Online]. Available: https://linkinghub.elsevier.com/retrieve/pii/S1389128621002061

[22] J. Wytrebowicz, K. Cabaj, and J. Krawiec, "Messaging protocols for IoT systems—A pragmatic comparison," *Sensors*, vol. 21, no. 20, p. 6904, Oct. 2021. [Online]. Available: https://www.mdpi.com/1424-8220/21/20/6904

[23] J. Schmidhuber, D. Wierstra, M. Gagliolo, and F. Gomez, "Training recurrent networks by evolino," *Neural Comput.*, vol. 19, no. 3, pp. 757–779, Mar. 2007. [Online]. Available: https://direct.mit.edu/neco/article/19/3/757-779/7156

[24] K. P. Tran, H. D. Nguyen, and S. Thomassey, "Anomaly detection using long short term memory networks and its applications in supply chain management," *IFAC-PapersOnLine*, vol. 52, no. 13, pp. 2408–2412, 2019.

[25] P. Palacios Játiva, M. Román Cañizares, C. A. Azurdia-Meza, D. Zabala-Blanco, A. D. Firoozabadi, F. Seguel, S. Montejo-Sánchez, and I. Soto, "Interference mitigation for visible light communications in underground mines using angle diversity receivers," *Sensors*, vol. 20, no. 2, p. 367, Jan. 2020. [Online]. Available: https://www.mdpi.com/1424-8220/20/2/367

[26] J. Wang, A. Al-Kinani, J. Sun, W. Zhang, and C.-X. Wang, "A path loss channel model for visible light communications in underground mines," in *Proc. IEEE/CIC Int. Conf. Commun. China (ICCC)*, Oct. 2017, pp. 1–5.

[27] I. M. Mansour, "Effective visible light communication system for underground mining industry," *Indonesian J. Electr. Eng. Informat. (IJEEI)*, vol. 8, no. 2, pp. 331–339, Jun. 2020. [Online]. Available: http://section.iaesonline.com/index.php/IJEEI/article/view/1978
[28] F. Javaid, A. Wang, M. U. Sana, A. Husain, and I. Ashraf, "Characteristic study of visible light communication and influence of coal dust particles in underground coal mines," *Electronics*, vol. 10, no. 8, p. 883, Apr. 2021. [Online]. Available: https://www.mdpi.com/2079-9292/10/8/883
[29] P. P. Játiva, C. A. Azurdia-Meza, I. Sánchez, F. Seguel, D. Zabala-Blanco, A. D. Firoozabadi, C. A. Gutiérrez, and I. Soto, "A VLC channel model for underground mining environments with scattering and shadowing," *IEEE Access*, vol. 8, pp. 185445–185464, 2020. [Online]. Available: https://ieeexplore.ieee.org/document/9222015/
[30] Z. Ahmed, L. Zhang, G. Faulkner, D. O'Brien, and S. Collins, "A shot-noise limited 420 mbps visible light communication system using commerical off-the-shelf silicon photomultiplier (SiPM)," in *Proc. IEEE Int. Conf. Commun. Workshops (ICC Workshops)*, May 2019, pp. 1–5. [Online]. Available: https://ieeexplore.ieee.org/document/8757030/
[31] H. Farahneh, C. Mekhiel, A. Khalifeh, W. Farjow, and X. Fernando, "Shadowing effects on visible light communication channels," in *Proc. IEEE Can. Conf. Electr. Comput. Eng. (CCECE)*, May 2016, pp. 1–5.
[32] J. Munoz-Saez, I. Soto, R. Zamorano-Illanes, D. Fuentealba, W. Kern, and S. Gutierrez, "A comparative analysis of 5G digital twin microservices with FSO integration for underground mining ventilation," in *Proc. South Amer. Conf. Visible Light Commun. (SACVLC)*, Nov. 2023, pp. 82–87. [Online]. Available: https://ieeexplore.ieee.org/document/10347734/

PABLO PALACIOS JÁTIVA (Member, IEEE) received the B.S. degree in electronics and telecommunications engineering from the Escuela Superior Politécnica del Litoral (ESPOL), Guayaquil, Ecuador, in 2013, and the master's degree in communications network engineering and the Ph.D. degree in electrical engineering from the University of Chile, Santiago, Chile, in 2017 and 2023, respectively. He is currently a Professor with Universidad Diego Portales, Santiago. His current research interests include modeling, design, and performance analysis of optical wireless communication; and RF communication systems. He has served as a technical program committee (TPC) member and a reviewer for multiple conferences. He was a Reviewer of journals, such as IEEE Access, IEEE Internet of Things Journal, and *IEEE Communications Magazine*.

ISMAEL SOTO (Member, IEEE) was born in Punta Arenas, Chile. He received the degree in engineering from the University of Santiago of Chile, in 1982, the Master of Engineering degree from University Federico Santa Maria, in 1990, and the Ph.D. degree from the University of Staffordshire, U.K., in 1997. He has taught with the Department of Computer Science, Department of Industrial Engineering, and Department of Electrical Engineering, University of Santiago of Chile, where he is currently an Associate Professor of telecommunications and signal processing with the Electrical Engineering Department. He has been the National Director and a member of the International Speech Communication Association. He has participated in several national and international research projects on radio and visible light communication technology. He registers patents in several countries. His research interests include safety, DSP, visible light communications, and big data. He received the Innovation Award from the Association of Electrical Engineers (AIE). He has been an ITC of CSNDSP and the Chairman of the Organizing Committee of SACVLC. He has been a Reviewer of multiple journals, such as *Optimization*, *IET Communications*, and *Optik*.

CESAR A. AZURDIA-MEZA (Member, IEEE) received the B.Sc. degree in electronics engineering from the Universidad del Valle de Guatemala, Guatemala, in 2005, the M.Sc. degree in electrical engineering from Linnaeus University, Sweden, in 2009, and the Ph.D. degree in electronics and radio engineering from Kyung Hee University, Republic of Korea, in 2013. He joined the Department of Electrical Engineering, University of Chile, as an Assistant Professor, in August 2013, and since August 2021, he has been an Associate Professor. His research interests include Nyquist's ISI criterion, OFDM-based systems, VLC systems, vehicular communications, and 5G and beyond enabling technologies. He is a member of the IEEE Communications Society and the IEICE Communications Society. He was a co-recipient of the 2019 IEEE LATINCOM Best Paper Award and the 2016 IEEE CONESCAPAN Best Paper Award. He was a supervisor of the awarded Ph.D. Thesis with the 2022 Abertis Award for Research in Road Safety (Ex-Aequo) at the national and international level.

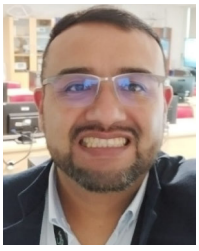

IVÁN SÁNCHEZ (Member, IEEE) received the Engineering degree from the National Polytechnic School of Ecuador, in 2006, and the M.Eng. degree from the Central University of Ecuador, in 2015. He is currently pursuing the Ph.D. degree with the University of Malaga, Spain. He is a Professor with the Universidad de Las Américas, Ecuador. His research interests include digital communications, electronic circuits, and electromagnetic theory.

RIU WANG received the Ph.D. degree from Shanghai Jiao Tong University, China, in 2013. From August 2012 to February 2013, he was a Visiting Ph.D. Student with the Department of Electrical Engineering, University of California, Riverside. From October 2013 to October 2014, he was with the Institute of Network Coding, The Chinese University of Hong Kong, as a Postdoctoral Research Associate. From October 2014 to December 2016, he was with the College of Electronics and Information Engineering, Tongji University, as an Assistant Professor, where he is currently a Full Professor. He has published more than 70 articles. His research interests include wireless communications, artificial intelligence, and wireless positioning. He received the Shanghai Excellent Doctor Degree Dissertation Award, in 2015, and the ACM Shanghai Rising Star Nomination Award, in 2016.

WERTHER KERN received the first degree in agricultural engineer from the University of Chile, the second degree in industrial civil engineer from University Federico Santa María; the Master of Business Administration degree from Loyola College Maryland, the master's degree in business administration from ILADES, and the Dr. (Ph.D.) degree in management sciences from the University of Santiago of Chile. He was a former Professor with the University of Chile. He is an Advisor to private companies in matters related to project formulation, cost evaluation, and market intelligence studies. He is a Lecturer of courses of his specialty in diploma courses and courses aimed at training professionals in the private and public sector.